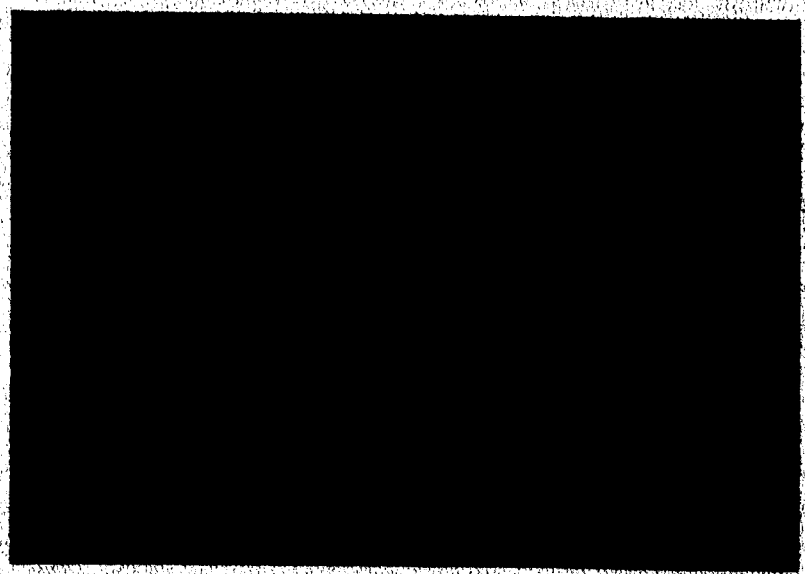


MECHANICAL
TECHNOLOGY
INCORPORATED

GPO PRICE \$ _____
CFSTI PRICE(S) \$ _____
Hard copy (HC) \$ 3.00
Microfiche (MF) 1.50
ff 653 July 65

N66 23677
(ACCESSION NUMBER)
51
(PAGES)
CR-71850
(NASA CR OR TMX OR AD NUMBER)
(THRU) _____
(CODE) 1
(CATEGORY) 15



MECHANICAL TECHNOLOGY INCORPORATED
968 Albany-Shaker Road
Latham, New York 12110

Task Report I on phase II
MTI-65TR30

SPHERICAL SQUEEZE-FILM HYBRID BEARING
WITH SMALL STEADY-STATE
RADIAL DISPLACEMENT

by

T. Chiang
S.B. Malanoski
C.H.T. Pan

November, 1965

TECHNICAL REPORT

SPHERICAL SQUEEZE-FILM HYBRID BEARING
WITH SMALL STEADY-STATE
RADIAL DISPLACEMENT

J. Chiang S. P. Malanowski C. H. T. Pan
Author (s)

E. B. Arwas.
Approved

Approved

Prepared under

Contract: NAS 8-11678

Prepared for

NATIONAL AERONAUTICS AND SPACE ADMINISTRATION
GEORGE C. MARSHALL SPACE FLIGHT CENTER
HUNTSVILLE, ALABAMA

Administered by

NATIONAL AERONAUTICS AND SPACE ADMINISTRATION
GEORGE C. MARSHALL SPACE FLIGHT CENTER
HUNTSVILLE, ALABAMA

MTI
MECHANICAL TECHNOLOGY INCORPORATED
MTI

968 ALBANY - SHAKER ROAD — LATHAM, NEW YORK — PHONE 785-0922

TABLE OF CONTENTS

	<u>Page</u>
ABSTRACT	ii
1. INTRODUCTION	1
2. ANALYSIS	2
2.1. Basic Equations	2
2.2. Asymptotic Approximation	3
2.3. Mass Content Rule	4
2.4. Perturbation Solution - small n_r	6
3. AXIALLY SYMMETRIC CASE	8
4. NON-AXIALLY SYMMETRIC CASE	10
5. INFLUENCE OF STRUCTURAL FLEXURE	14
6. RESULTS	17
7. CONCLUSIONS	19
ACKNOWLEDGEMENT	20
REFERENCES	21
APPENDIX I	22
APPENDIX II	25
NOMENCLATURE	28
LIST OF FIGURES	30

23677

ABSTRACT

Spherical squeeze-film hybrid bearings were analyzed theoretically. Based on an asymptotic approximation for large squeeze number, the solution of the Reynolds' equation applicable to the system under investigation was obtained. Perturbation method has been used; the results are valid for small radial displacement only. It has no limitation however in the values of compressibility number, axial displacement ratio and excursion ratio. Numerical calculations have been programmed on the GE205 computer. Axial load-capacity, axial stiffness and radial stiffness and attitude angle were obtained.

I. INTRODUCTION

In a gaseous squeeze-film bearing, one of the bearing surfaces is made to oscillate transversely. By virtue of this high frequency transverse oscillation of the bearing surface and the non-linear nature of the gaseous flow in the film, the time-averaged film pressure becomes greater than the ambient and, consequently, a load-carrying capacity is generated. To obtain a relatively large load capacity, it is desirable to have a high frequency and a relatively large transverse oscillation. This can be achieved by letting the oscillating bearing surface be part of a resonant transducer system. In the literature, theoretical and experimental investigations on gaseous squeeze-film bearing have been made. References 1 and 2 concerned journal and thrust bearings and Reference 5 provides the foundation for the analysis of squeeze-film bearings of arbitrary bearing shape and arbitrary mode of gap oscillations.

The purpose of the present investigation is to analyze spherical squeeze-film hybrid bearings with small radial displacement. Based on an asymptotic approximation for large squeeze number, the solution of the Reynolds' equation with an assumed mode of gap oscillation was obtained. The perturbation method has been used; the results are valid for small radial displacement only. The results obtained (axial load capacity, axial stiffness and radial and tangential stiffnesses) provide pertinent information in designing spherical squeeze-film bearings.

2. ANALYSIS

The squeeze-film bearing presently under consideration consists of two spherical surfaces, the geometry of which is shown in Figure 1. Spherical coordinates have been used - θ and ϕ are respectively the meridional and azimuthal angles. The bearing extends in the ϕ -direction from ϕ_1 to ϕ_2 .

2.1. Basic Equations

The isothermal Reynolds' equation of a spherical squeeze-film bearing with meridional journal angular speed ω and squeeze frequency Ω , is (Reference 3)

$$\begin{aligned} & \sin\phi \frac{\partial}{\partial\phi} \left[\sin\phi H^3 P \frac{\partial P}{\partial\phi} \right] + \frac{\partial}{\partial\theta} \left[H^3 P \frac{\partial P}{\partial\theta} \right] \\ & = \sin^2\phi \left[\Lambda \frac{\partial}{\partial\theta} + \sigma \frac{\partial}{\partial\tau} \right] (PH), \dots\dots\dots (2.1) \end{aligned}$$

where

$$\begin{aligned} \sigma &= \frac{12\mu\Omega}{P_a} \left(\frac{R}{C} \right)^2 = \text{Squeeze number} \\ \Lambda &= \frac{6\mu\omega}{P_a} \left(\frac{R}{C} \right)^2 = \text{Compressibility number} \dots\dots\dots (2.2) \\ \tau &= \Omega t = \text{Dimensionless time.} \end{aligned}$$

In this report it is assumed that the squeeze motion is entirely in the axial direction. Setting ϵ = excursion ratio, η_z , η_r = axial and radial displacement ratio respectively, the normalized film gap can be expressed as (Ref. 3)

$$H(\phi, \theta, \tau) = 1 + (\epsilon \cos\tau + \eta_z) \cos\phi + \eta_r \sin\phi \cos(\theta - \alpha) \dots\dots\dots (2.3)$$

The boundary conditions of equation (2.1) are

$$P(\phi_1, \theta, \tau) = P(\phi_2, \theta, \tau) = 1 \dots\dots\dots (2.4)$$

$$P(\phi, \theta, \tau) = P(\phi, \theta + 2\pi, \tau) \dots\dots\dots (2.5)$$

$$\left. \frac{\partial P}{\partial\theta} \right|_{\phi, \tau} = \left. \frac{\partial P}{\partial\theta} \right|_{\phi, \theta+2\pi, \tau} \dots\dots\dots (2.6)$$

plus the condition of periodicity in time,

$$P(\phi, \theta, \tau) = P(\phi, \theta, \tau + 2\pi) \dots\dots\dots (2.7)$$

2.2 Asymptotic Approximation

The squeeze number σ is generally very large. For $p_a = 14.7$ psia, $\frac{\mu}{\rho} = 1.7 \times 10^{-4} \text{ ft}^2/\text{sec}$, $\rho = 0.074 \text{ lb/ft}^3$, $\Omega = 40,000 \pi \text{ rad/sec}$, $\frac{R}{C} = 1000$, we have a typical value of σ -

$$\sigma = \frac{12\mu \Omega}{p_a} \left(\frac{R}{C} \right)^2 = 275.$$

Hence, the asymptotic solution ($\sigma \rightarrow \infty$) of equation (2.1) is of interest. A general treatment of squeeze-film bearings using the asymptotic method is given in Ref. 5. The analysis to be developed is a special application of this method to spherical bearings. Rewrite equation (2.1)

$$\frac{\partial}{\partial \tau} (PH) = \frac{1}{\sigma \sin^2 \varphi} \left\{ \sin \varphi \frac{\partial}{\partial \varphi} \left[\sin \varphi H^3 P \frac{\partial P}{\partial \varphi} \right] + \frac{\partial}{\partial \theta} \left[H^3 P \frac{\partial P}{\partial \theta} - \Lambda \sin^2 \varphi (PH) \right] \right\} \quad (2.8)$$

$$\text{As } \sigma \rightarrow \infty, \frac{\partial}{\partial \tau} (PH) = 0 \quad (2.9)$$

$$\text{Denoting } \psi \equiv PH \quad (2.10)$$

we have

$$\text{as } \sigma \rightarrow \infty, \psi = \psi_{\infty}(\varphi, \theta) \quad (2.11)$$

except in the boundary layers near $\varphi = \varphi_1$, and $\varphi = \varphi_2$. The extent of the boundary layers is of the order of $\sigma^{-1/2}$. Let ψ_e be an edge correction in the boundary layer, then

$$\psi = \psi_e(\varphi, \theta, \tau) + \psi_{\infty}(\varphi, \theta) \quad (2.12)$$

During the process of reduction from equation (2.8) to equation (2.9), the differential equation loses two orders in φ -differentiation; consequently the asymptotic solution ψ_{∞} will not satisfy the two boundary conditions (2.4). The boundary conditions to be satisfied by ψ_{∞} at φ_1 and φ_2 can only be determined by a mass content rule which will be discussed later.

Using the identity

$$H^3 P \, dP = 1/2 \, d(H \psi^2) - 3/2 \, \psi^2 \, dH \quad (2.13)$$

and integrating (2.8) with respect to τ from 0 to 2π , we obtain

$$\int_0^{2\pi} \sin \varphi \frac{\partial}{\partial \varphi} \left[\sin \varphi \frac{\partial}{\partial \varphi} (H \psi^2) - 3\psi^2 \sin \varphi \frac{\partial H}{\partial \varphi} \right] d\tau$$

$$\int_0^{2\pi} \frac{\partial}{\partial \theta} \left[\frac{\partial}{\partial \theta} (H \psi^2) - 3\psi^2 \frac{\partial H}{\partial \theta} - 2\Lambda \sin^2 \varphi \psi \right] d\tau = 0 \quad (2.14)$$

Using the asymptotic approximation (2.11) and neglecting the edge correction ψ_e ,

equation (2.14) is readily reduced to:

$$\sin \frac{\partial}{\partial \varphi} \left[\sin \frac{\partial}{\partial \varphi} (H_0 \psi_\infty^2) - 3 \psi_\infty \sin \varphi \frac{\partial H_0}{\partial \varphi} \right] + \frac{\partial}{\partial \theta} \left[\frac{\partial}{\partial \theta} (H_0 \psi_\infty^2) - 3 \psi_\infty^2 \frac{\partial H_0}{\partial \theta} - 2 \Lambda \sin^2 \varphi \psi_\infty \right] = 0 \quad (2.15)$$

$$\text{where } H_0 = 1 + \eta_z \cos \varphi + \eta_r \sin \varphi \cos (\theta - \alpha) \quad (2.16)$$

which is the time average of H given by Eq. (2.3).

The θ - wise boundary conditions require that both ψ_∞ and its derivative be periodic in θ ,

$$\psi_\infty (\varphi, \theta) = \psi_\infty (\varphi, \theta + 2\pi) \quad (2.17)$$

$$\left. \frac{\partial \psi_\infty}{\partial \theta} \right|_{\varphi, \theta} = \left. \frac{\partial \psi_\infty}{\partial \theta} \right|_{\varphi, \theta + 2\pi} \quad (2.18)$$

The φ -wise boundary conditions, however, are not known explicitly. Eq. (2.4) is not useful because at φ_1 and φ_2 the edge correction (ψ_e) is important, but unknown.

In the following section a mass content rule will be derived which may be used as boundary conditions for ψ_∞ at φ_1 and φ_2 .

2.3 Mass Content Rule

In deriving the Mass Content Rule, the method used here is quite similar to those in Reference 4 which deals with the axially symmetric problem. We shall proceed by integrating Eq. (2.14) with respect to φ ,

$$\int_0^{2\pi} d\tau \sin \varphi \left[\frac{\partial}{\partial \varphi} (H \psi^2) - 3 \psi^2 \frac{\partial H}{\partial \varphi} \right] + \int_{\varphi_1}^{\varphi} \frac{d\varphi'}{\sin \varphi'} \int_0^{2\pi} d\tau \frac{\partial}{\partial \theta} \left[\frac{\partial}{\partial \theta} (H \psi^2) - 3 \psi^2 \frac{\partial H}{\partial \theta} \right]$$

Integrating once again, we obtain

$$\int_0^{2\pi} H \psi^2 d\tau = A(\theta) \int_{\varphi_1}^{\varphi} \frac{d\varphi'}{\sin \varphi'} + B(\theta) + I(\varphi, \theta) \quad (2.19)$$

where $A(\theta)$ and $B(\theta)$ are "constants" of integration,

$$\begin{aligned} \text{and } I(\varphi, \theta) = & 3 \int_{\varphi_1}^{\varphi} d\varphi' \int_0^{2\pi} d\tau \left[\psi(\varphi', \theta, \tau) \right]^2 \frac{\partial H(\varphi', \theta, \tau)}{d\varphi'} \\ & - \int_{\varphi_1}^{\varphi} \frac{d\varphi''}{\sin \varphi} \int_{\varphi_1}^{\varphi''} \frac{d\varphi'}{\sin \varphi'} \int_0^{2\pi} d\tau \frac{\partial}{\partial \theta} \left\{ \frac{\partial}{\partial \theta} \left[H(\varphi', \theta, \tau) \psi^2(\varphi', \theta, \tau) \right] \right\} \end{aligned}$$

$$- 3\psi^2 (\varphi', \theta, \tau) \frac{\partial H(\varphi', \theta, \tau)}{\partial \theta} \Bigg\} \quad (2.20)$$

On the boundary, $\varphi = \varphi_i$ ($i = 1, 2$), and $P(\varphi_i, \theta, \tau) = 1$.

$$\text{Thus, } \psi(\varphi_i, \theta, \tau) = H(\varphi_i, \theta, \tau) \quad \dots \dots \dots (2.21)$$

and Equation (2.19) becomes

$$\int_0^{2\pi} H^3(\varphi_i, \theta, \tau) d\tau = A(\theta) \int_{\varphi_1}^{\varphi_i} \frac{d\varphi'}{\sin\varphi'} + B(\theta) + I(\varphi_i, \theta) \quad \dots \dots \dots (2.22)$$

($i = 1, 2$)

On the left hand side of Eq. (2.19) replace ψ by ψ_∞

$$\psi_\infty^2(\varphi, \theta) \int_0^{2\pi} H d\tau = A(\theta) \int_{\varphi_1}^{\varphi} \frac{d\varphi'}{\sin\varphi'} + B(\theta) + I(\varphi, \theta) \quad \dots \dots \dots (2.23)$$

($\varphi \neq \varphi_i$)

Let the boundary layer thickness at φ_1 be $\delta\varphi_1$, then Eq.(2.23) can be evaluated at $\varphi = \varphi_1 + \delta\varphi_1$.

$$\psi_\infty^2(\varphi_1 + \delta\varphi_1, \theta) \int_0^{2\pi} H(\varphi_1 + \delta\varphi_1, \theta, \tau) d\tau = A(\theta) \int_{\varphi_1}^{\varphi_1 + \delta\varphi_1} \frac{d\varphi'}{\sin\varphi'} + B(\theta) + I(\varphi_1 + \delta\varphi_1, \theta) \quad \dots \dots \dots (2.24)$$

Since $\delta\varphi_1$ is of the order of $(\sigma^{-\frac{1}{2}})$, the right-hand sides of (2.22) with $i = 1$, and (2.24) are equal (neglecting $O(\sigma^{-\frac{1}{2}})$).

Hence a comparison of (2.22) and (2.24) leads to

$$\int_0^{2\pi} H^3(\varphi_1, \theta, \tau) d\tau = \psi_\infty^2(\varphi_1 + \delta\varphi_1, \theta) \int_0^{2\pi} H(\varphi_1 + \delta\varphi_1, \theta, \tau) d\tau \quad \dots \dots \dots (2.25)$$

Again, because $\delta\varphi_1$ is small it is reasonable to assume

$$\psi_\infty(\varphi_1 + \delta\varphi_1, \theta) = \psi_\infty(\varphi_1, \theta). \text{ Hence}$$

$$\psi_\infty^2(\varphi_1, \theta) = \frac{\int_0^{2\pi} H^3(\varphi_1, \theta, \tau) d\tau}{2\pi H_0(\varphi_1, \theta)} \quad \dots \dots \dots (2.26)$$

Similarly,

$$\psi_\infty^2(\varphi_2, \theta) = \frac{\int_0^{2\pi} H^3(\varphi_2, \theta, \tau) d\tau}{2\pi H_0(\varphi_2, \theta)} \quad \dots \dots \dots (2.27)$$

The mass content rules (2.26) and (2.27) provide boundary conditions for ψ_∞ at φ_1 and φ_2 .

2.4. Perturbation Solution - small η_r

The asymptotic solution ψ_∞ governed by Equation (2.15) will be solved in this section. The pertinent boundary conditions are (2.17), (2.18), (2.26.) and (2.27.) For small radial displacement ratio (η_r) the problem can be solved by perturbation method. It is convenient to expand

$$H_o \psi_\infty^2 = g_o(\varphi) + \eta_r \operatorname{Re} \left\{ g_1(\varphi) e^{i\bar{\theta}} \right\} \dots \dots \dots (2.28)$$

$$\text{where } \bar{\theta} = \theta - \alpha \dots \dots \dots (2.29)$$

Note that $g_1(\varphi)$ may be complex. The zeroth-order solution $g_o(\varphi)$ is a function of φ only, since for zero radial displacement $H_o \psi_\infty^2$ should be independent of θ .

Rewrite (2.16) in the form

$$H_o(\varphi, \theta) = h_o(\varphi) + \eta_r \operatorname{Re} \left\{ h_1(\varphi) e^{i\bar{\theta}} \right\} \dots \dots \dots (2.30)$$

$$\text{where } h_o(\varphi) = 1 + \eta_z \cos \varphi \dots \dots \dots (2.31)$$

$$h_1(\varphi) = \sin \varphi \dots \dots \dots (2.32)$$

Substituting Eqs. (2.28) and (2.30) into eq. (2.15) we obtain

$$\eta_r^0 : \sin \varphi \frac{d}{d\varphi} \left[\sin \varphi \left(\frac{dg_o}{d\varphi} - 3 \frac{g_o}{h_o} \frac{dh_o}{d\varphi} \right) \right] = 0 \dots \dots \dots (2.33)$$

$$\eta_r^1 : \sin \varphi \frac{d}{d\varphi} \left\{ \sin \varphi \left[\frac{dg_1}{d\varphi} - 3 \frac{g_1}{h_o} \frac{dh_o}{d\varphi} - 3 g_o \frac{d}{d\varphi} \left(\frac{h_1}{h_o} \right) \right] \right\}$$

$$- g_1 + 3 \frac{g_o}{h_o} h_1 - i \Lambda \sin^2 \varphi \sqrt{\frac{g_o}{h_o}} \left(\frac{g_1}{g_o} - \frac{h_1}{h_o} \right) = 0 \dots \dots \dots (2.34)$$

The boundary conditions (2.26) and (2.27) can be integrated to give

$$\psi_\infty^2(\varphi_i, \theta) = \frac{\int_0^{2\pi} H^3(\varphi_i, \theta, \tau) d\tau}{2\pi H_o(\varphi_i, \tau)} \quad (i = 1, 2)$$

$$= H_o^2(\varphi_i, \theta) + \frac{3}{2} \epsilon^2 \cos^2 \varphi_i \dots \dots \dots (2.35)$$

Multiply both sides by $H_o (\varphi_i, \theta)$

$$g_o (\varphi_i) + \eta_r g_1 (\varphi_i) e^{i\bar{\theta}} = h_o^3 (\varphi_i) + \eta_r 3 h_o^2 (\varphi_i) h_1 (\varphi_i) e^{i\bar{\theta}} + \frac{3}{2} \epsilon^2 \cos^2 \varphi_i \left[h_o (\varphi_i) + \eta_r h_1 (\varphi_i) e^{i\bar{\theta}} \right], \quad (2.36)$$

which results in the following boundary conditions

$$g_o (\varphi_i) = h_o^3 (\varphi_i) + \frac{3}{2} \epsilon^2 h_o (\varphi_i) \cos^2 \varphi_i \quad (i = 1, 2) \dots \dots \dots (2.37)$$

$$g_1 (\varphi_i) = 3 h_o^2 (\varphi_i) h_1 (\varphi_i) + \frac{3}{2} \epsilon^2 h_1 (\varphi_i) \cos^2 \varphi_i \quad (i = 1, 2) \dots \dots \dots (2.38)$$

Thus, the solution of $H_o \psi_\infty^2$ is represented by $g_o(\varphi)$ and $g_1(\varphi)$ as indicated in (2.28). The zeroth-order solution $g_o(\varphi)$ representing the zero radial displacement problem can be obtained from Eq. (2.33) and boundary conditions (2.37). Having obtained $g_o(\varphi)$ from the above system, the first-order perturbation solution $g_1(\varphi)$ can readily be solved from differential Equation (2.34) and boundary conditions (2.38).

3. AXIALLY SYMMETRIC CASE

Spherical squeeze-film bearing with axial displacement only is considered in this section. The normalized film gap is given by Eq. (2.3). Thus, with $\eta_r = 0$, we have

$$H(\varphi, \theta) = h_o(\varphi) + \epsilon \cos\varphi \cos\tau \quad (3.1)$$

$$\text{where } h_o(\varphi) = 1 + \eta_z \cos\varphi \quad (2.31)$$

and $H_o(\varphi, \theta)$ reduces to $h_o(\varphi)$ as can be seen by Eq. (2.30).

Denoting the solution of ψ_∞^2 by G_o for the axially symmetric problem, it is clear from Eq. (2.28) that

$$g_o(\varphi) = h_o(\varphi) G_o(\varphi), \quad (3.2)$$

and G_o satisfies

$$\sin\varphi \frac{d}{d\varphi} \left[\sin\varphi \left(\frac{d}{d\varphi} (h_o G_o) - 3 G_o \frac{dh_o}{d\varphi} \right) \right] = 0, \quad (3.3)$$

with boundary conditions

$$G_o(\varphi_i) = h_o^2(\varphi_i) + \frac{3}{2} \epsilon^2 \cos^2 \varphi_i \quad (i = 1, 2) \quad (3.4)$$

Equations (3.3) and (3.4) can be readily deduced from (2.33), (2.37) and (3.2).

Eq. (3.3) can be integrated directly to yield

$$\sin\varphi \left[\frac{d}{d\varphi} (h_o G_o) - 3 G_o \frac{dh_o}{d\varphi} \right] = A \quad (3.5)$$

The solution to Eq. (3.5) can be obtained directly by assuming $G_o = h_o^2 F(\varphi)$ and substituting this expression into Eq. (3.5). Thus,

$$h_o^3 \frac{dF}{d\varphi} = \frac{A}{\sin\varphi} \quad (3.6)$$

Integrating Eq. (3.6) one obtains

$$F(\varphi) = A \int \frac{d\varphi}{\sin\varphi h_o^3} + F(\varphi_1), \quad (3.7)$$

where $F(\varphi_1) = (G_o/h_o^2)_1$.

With Eq. (3.7) and the assumption made above that $G_o = h_o^2 F(\varphi)$, one can write the solution for G_o and thus ψ_∞^2 .

$$G_o = \psi_\infty^2 = A h_o^2 \int_{\varphi_1} \frac{d\varphi}{\sin \varphi h_o^3} + \left[\frac{h_o(\varphi)}{h_o(\varphi)_1} \right]^2 \psi_\infty^2(\varphi_1) \dots \dots \dots (3.8)$$

By evaluating $\psi_\infty(\varphi)$ at φ_2 one obtains an expression for "A", thus,

$$A = \frac{\psi_\infty^2(\varphi_2) - \left[\frac{h_o(\varphi_2)}{h_o(\varphi_1)} \right]^2 \psi_\infty^2(\varphi_1)}{h_o^2(\varphi_2) \int_{\varphi_1}^{\varphi_2} \frac{d\varphi}{\sin \varphi h_o^3}} \dots \dots \dots (3.9)$$

The solution to the problem of the axially symmetric case is now complete. It is given by Eqs. (3.8), (3.9) and (3.4).

The pressure distribution for the asymptotic problem (large σ) is obtained from

$$P - p_a = p_a (P - 1) = p_a \left[\frac{\psi_\infty}{H} - 1 \right] \dots \dots \dots (3.10)$$

The mean axial load is

$$\begin{aligned} \frac{F_z}{\pi p_a R^2} &= \frac{1}{2\pi} \int_{\varphi_1}^{\varphi_2} d\varphi \int_0^{2\pi} \left(\frac{\psi_\infty}{H} - 1 \right) \sin 2\varphi d\tau, \\ \text{or} \quad &= \int_{\varphi_1}^{\varphi_2} \frac{\psi_\infty(\varphi) \sin 2\varphi d\varphi}{\sqrt{h_o^2 - \epsilon^2 \cos^2 \varphi}} + \frac{1}{2} [\cos 2\varphi_2 - \cos 2\varphi_1] \dots \dots \dots (3.11) \end{aligned}$$

The mean axial stiffness is

$$\begin{aligned} \frac{Ck_z}{\pi p_a R^2} &= - \frac{\partial}{\partial \eta_z} \left(\frac{F_z}{\pi p_a R^2} \right) \\ &= - \frac{1}{2\pi} \int_{\varphi_1}^{\varphi_2} d\varphi \int_0^{2\pi} \frac{\partial}{\partial \eta_z} \left(\frac{\psi_\infty}{H} \right) \sin 2\varphi d\tau \dots \dots \dots (3.12) \end{aligned}$$

Above expressions can be further reduced analytically for specific geometries. Some of these are given in Appendix I.

4. NON-AXIALLY SYMMETRIC CASE

Having solved the axially symmetric problem and knowing its solution $g_0(\varphi)$ from Section 3, we are in a position to solve the non-axially symmetric problem, i.e. there is a small radial eccentricity. By perturbation method, the governing differential equation of $g_1(\varphi)$ and boundary conditions have been obtained in Section 2.4.; they are respectively Eqs. (2.34) and (2.38). Since $g_1(\varphi)$ may be complex, we assume

$$g_1(\varphi) = u(\varphi) + i v(\varphi) \quad \dots \dots \dots (4.1)$$

Using Eq. (4.1) and separating the real and imaginary parts of Equations (2.34) and (2.38), we obtain

$$\begin{aligned} \sin\varphi \frac{d}{d\varphi} \left(\sin\varphi \frac{du}{d\varphi} \right) - 3 \sin\varphi \frac{d}{d\varphi} \left(\frac{u \sin\varphi}{h_0} \frac{dh_0}{d\varphi} \right) - u + \Lambda \sin^2\varphi \sqrt{\frac{g_0}{h_0}} \frac{v}{g_0} \\ = 3 \sin\varphi \frac{d}{d\varphi} \left[\sin\varphi g_0 \frac{d}{d\varphi} \left(\frac{h_1}{h_0} \right) \right] - 3 \frac{g_0}{h_0} h_1 \quad \dots \dots \dots (4.2) \end{aligned}$$

$$\begin{aligned} - \Lambda \sin^2\varphi \sqrt{\frac{g_0}{h_0}} \frac{u}{g_0} + \sin\varphi \frac{d}{d\varphi} \left(\sin\varphi \frac{dv}{d\varphi} \right) - 3 \sin\varphi \frac{d}{d\varphi} \left(\frac{v \sin\varphi}{h_0} \frac{dh_0}{d\varphi} \right) - v \\ = - \Lambda \sin^2\varphi \sqrt{\frac{g_0}{h_0}} \frac{h_1}{h_0}, \quad \dots \dots \dots (4.3) \end{aligned}$$

with boundary conditions

$$\begin{aligned} u(\varphi_i) = 3 h_1(\varphi_i) \left[h_0^2(\varphi_i) + \frac{1}{2} \epsilon^2 \cos^2 \varphi_i \right] \\ v(\varphi_i) = 0 \quad (i = 1, 2) \quad \dots \dots \dots (4.4) \end{aligned}$$

Equations (4.2) and (4.3) are two simultaneous second order ordinary differential equations, and Equation (4.4) provides four boundary conditions which are required to solve the above Equations. The solutions (u and v) of Eqs. (4.2) and (4.3) based on numerical integration using "influence coefficient" method is shown in Appendix II.

Knowing u and v , the pressure distribution for large σ may be obtained from Eqs. (2.10) and (2.28).

$$P = \sqrt{\frac{H_0 \psi_\infty^2}{H_0 H^2}} \quad \dots \dots \dots (4.5)$$

or,

$$P = \frac{\sqrt{G_o}}{h_o + \epsilon \cos \varphi \cos \tau} + \eta_r \left\{ \frac{1}{h_o + \epsilon \cos \varphi \cos \tau} \left[\frac{u \cos \bar{\theta} - v \sin \bar{\theta}}{2 h_o \sqrt{G_o}} - \frac{\sqrt{G_o} h_1 \cos \bar{\theta}}{2 h_o} \right] - \frac{\sqrt{G_o} h_1 \cos \bar{\theta}}{(h_o + \epsilon \cos \varphi \cos \tau)^2} \right\} \quad (4.6)$$

It is interesting to note that although the product of PH , ψ , is time-independent for large σ , the pressure P however, is a function of time through the relationship $P = \psi_{\infty}/H$. The pressure as expressed by Eq. (4.6) consists of an axially symmetric term plus a perturbation term due to radial displacement.

To obtain bearing forces we first take the time average of P , then integrate throughout the bearing film. Denoting the axial, radial and tangential forces by F_Z , F_R and F_T , respectively,

Axial Force

$$F_Z = \int_{\varphi_1}^{\varphi_2} d\varphi \int_0^{2\pi} \frac{d\tau}{2\pi} \int_0^{2\pi} (p - p_a) \cos \varphi \sin \varphi R^2 d\theta \quad (4.7)$$

and

$$\frac{F_Z}{\pi R^2 p_a} = \frac{1}{4\pi^2} \int_{\varphi_1}^{\varphi_2} d\varphi \int_0^{2\pi} d\tau \int_0^{2\pi} (P - 1) \sin 2\varphi d\theta \quad (4.8)$$

Radial Force

$$F_R = \int_{\varphi_1}^{\varphi_2} \int_{\theta=0}^{2\pi} \int_{\tau=0}^{2\pi} (p - p_a) \sin \varphi (-\cos \bar{\theta}) R \sin \varphi d\theta R d\varphi \frac{d\tau}{2\pi} \quad (4.9)$$

Since the radial displacement problem is linearized, the radial force per unit deflection is the radial stiffness. Normalizing, the radial stiffness is

$$\frac{Ck_R}{\pi R^2 p_a} = \frac{F_R}{\pi R^2 p_a \eta_R} = - \frac{1}{2\pi^2 \eta_r} \int_0^{2\pi} \cos \bar{\theta} d\theta \int_{\varphi_1}^{\varphi_2} \sin^2 \varphi d\varphi \int_0^{2\pi} (P - 1) d\tau \quad (4.10)$$

Tangential Force

$$F_T = \int_{\varphi_1}^{\varphi_2} \int_{\theta=0}^{2\pi} \int_{\tau=0}^{2\pi} (p - p_a) \sin \varphi (\sin \bar{\theta}) R \sin \varphi d\theta R d\varphi \frac{d\tau}{2\pi} \quad (4.11)$$

Defining the tangential force per unit radial displacement as the tangential stiffness and normalizing as above, we have

$$\frac{Ck_T}{\pi R^2 p_a} = \frac{F_T}{\pi R^2 p_a \eta_T} = \frac{1}{2\pi^2 \eta_T} \int_0^{2\pi} \sin \bar{\theta} d\theta \int_{\phi_1}^{\phi_2} \sin^2 \phi d\phi \int_0^{2\pi} (P-1) d\tau \dots (4.12)$$

Performing the θ - integration in Eq. (4.8) and using Eq. (4.6) we have

$$\frac{F_Z}{\pi R^2 p_a} = \frac{1}{2\pi} \int_{\phi_1}^{\phi_2} d\phi \int_0^{2\pi} \left\{ \frac{\sqrt{G_o}}{h_o + \epsilon \cos \phi \cos \tau} - 1 \right\} \sin 2\phi d\tau \dots (4.13)$$

Since the perturbation term drops out in θ - integration due to symmetry, the axial force is indifferent of small radial eccentricity. Integrating Eq. (4.13) with respect to τ

$$\frac{F_Z}{\pi R^2 p_a} = \int_{\phi_1}^{\phi_2} \frac{\sqrt{G_o} \sin 2\phi d\phi}{\sqrt{h_o^2 - \epsilon^2 \cos^2 \phi}} + \frac{1}{2} \left[\cos 2\phi_2 - \cos 2\phi_1 \right] \dots (4.14)$$

We have used Eq. (309) of Reference [6]

$$\int_0^{2\pi} \frac{d\tau}{a+b \cos \tau} = \frac{2\pi}{\sqrt{a^2 - b^2}} \dots (4.15)$$

As may be anticipated Eq. (4.14) is identical to Eq. (3.11).

Equation (3.7) of Reference [6] is also useful.

$$\int_0^{2\pi} \frac{d\tau}{(a+b \cos \tau)^2} = \frac{a}{a^2 - b^2} \int_0^{2\pi} \frac{d\tau}{a+b \cos \tau} = \frac{2\pi a}{(a^2 - b^2)^{3/2}} \dots (4.16)$$

The dimensionless radial and tangential forces of (4.10) and (4.12) can be similarly reduced to

$$\frac{Ck_R}{\pi R^2 p_a} = \int_{\phi_1}^{\phi_2} \frac{\sin^2 \phi}{\sqrt{h_o^2 - \epsilon^2 \cos^2 \phi}} \left\{ \frac{u - G_o h_1}{2\sqrt{G_o} h_o} - \frac{\sqrt{G_o} h_o h_1}{h_o^2 - \epsilon^2 \cos^2 \phi} \right\} d\phi \dots (4.17)$$

$$\frac{Ck_T}{\pi R^2 p_a} = - \int_{\phi_1}^{\phi_2} \frac{\sin^2 \phi}{\sqrt{h_o^2 - \epsilon^2 \cos^2 \phi}} \frac{v}{2 h_o \sqrt{G_o}} d\phi \dots \dots \dots (4.18)$$

With the solutions u and v obtained by the method described in Appendix II, we may calculate (4.17) and (4.18) numerically.

5. INFLUENCE OF STRUCTURAL FLEXURE

Analyses of previous sections considered a spherical squeeze-film bearing with squeeze motion uniformly in the axial direction; the bearing was assumed to be rigid.

Due to structural flexibility the bearing tends to vibrate at frequency synchronous with the excursion frequency. An axially symmetrical mode of vibrations is assumed. Thus, the normalized film gap may be expressed by

$$\tilde{H}(\varphi, \theta, \tau) = H_0(\varphi, \theta) + \epsilon \cos \varphi \cos \tau + b(\varphi) \cos \tau \quad \dots \dots \dots (5.1)$$

The last term of Eq. (5.1) represents the contribution due to axially symmetrical synchronous structural vibrations. $b(\varphi)$ is related to the mode shape of vibrations.

The asymptotic analysis and the Mass Content Rule derived in Section 2 are still applicable here if H is replaced by \tilde{H} . Denote each quantity q which needs to be modified due to structural vibrations, by \tilde{q} . Thus

$$\tilde{\psi} = \tilde{P} \tilde{H} \quad \dots \dots \dots (5.2)$$

The differential equation for $\tilde{\psi}_\infty$ which is the asymptotic approximation of ψ for large σ , is

$$\begin{aligned} & \sin \varphi \frac{\partial}{\partial \varphi} \left[\sin \frac{\partial}{\partial \varphi} (H_0 \tilde{\psi}_\infty^2) - 3 \tilde{\psi}_\infty^2 \sin \varphi \frac{\partial H_0}{\partial \varphi} \right] \\ & + \frac{\partial}{\partial \theta} \left[\frac{\partial}{\partial \theta} (H_0 \tilde{\psi}_\infty^2) - 3 \tilde{\psi}_\infty^2 \frac{\partial H_0}{\partial \theta} - 2\Lambda \sin^2 \varphi \tilde{\psi}_\infty \right] = 0 \quad \dots \dots \dots (5.3) \end{aligned}$$

Eq. (5.3) is of the same form of Eq. (2.15).

Using the mass content rule of Section 2.3., we have

$$\tilde{\psi}_\infty^2(\varphi_i, \theta) = \frac{\int_0^{2\pi} \tilde{H}^3(\varphi_i, \theta, \tau) d\tau}{2\pi H_0(\varphi_i, \theta)} \quad (i = 1, 2) \quad \dots \dots \dots (5.4)$$

Substituting Eq. (5.1) into Eq. (5.4) results in

$$\tilde{\psi}_\infty^2(\varphi_i, \theta) = H_0^2(\varphi_i, \theta) + \frac{3}{2} \left[\epsilon \cos \varphi_i + b(\varphi_i) \right]^2 \quad (i = 1, 2) \quad \dots \dots \dots (5.5)$$

Equation (5.5) serves as two boundary conditions in the φ direction. Therefore, it is seen that in the analyses the only modification required due to structure vibration is in the φ -wise boundary conditions.

For small radial displacement apply perturbation method and expand

$$H_o \tilde{\psi}_\infty^2 = \tilde{g}_o(\varphi) + \eta_r \left\{ \text{Re } \tilde{g}_1(\varphi) e^{i\theta} \right\} \dots \dots \dots (5.6)$$

Substitution of Eq. (5.6.) into Eq. (5.3.) results in the same equations as (2.33) and (2.34) upon replacing $g_o(\varphi)$ and $g_1(\varphi)$ by $\tilde{g}_o(\varphi)$ and $\tilde{g}_1(\varphi)$ respectively. From Eq. (5.5) the boundary conditions are readily deduced,

$$\tilde{g}_o(\varphi_i) = h_o^3(\varphi_i) + \frac{3}{2} h_o(\varphi_i) \left[\epsilon \cos \varphi_i + b(\varphi_i) \right]^2 \quad (i = 1, 2) \dots \dots \dots (5.7)$$

$$\tilde{g}_1(\varphi_i) = 3 h_o^2(\varphi_i) h_1(\varphi_i) + \frac{3}{2} h_1(\varphi_i) \left[\epsilon \cos \varphi_i + b(\varphi_i) \right]^2 \quad (i = 1, 2) \dots \dots \dots (5.8)$$

It can be shown, following exactly the same procedures as developed in Section 3, that the solution to the axially symmetrical problem is given by

$$\tilde{G}_o = \tilde{\psi}_\infty^2 = \tilde{A} h_o^2(\varphi) \int_{\varphi_1}^{\varphi} \frac{d\varphi'}{\sin \varphi' h_o^3(\varphi')} + \tilde{B} h_o^2(\varphi) \dots \dots \dots (5.9)$$

where

$$\tilde{A} = \frac{3}{2} \frac{\left[\frac{\epsilon \cos \varphi_2 + b(\varphi_2)}{h_o(\varphi_2)} \right]^2 - \left[\frac{\epsilon \cos \varphi_1 + b(\varphi_1)}{h_o(\varphi_1)} \right]^2}{\int_{\varphi_1}^{\varphi_2} \frac{d\varphi}{\sin \varphi [h_o(\varphi)]^3}} \dots \dots \dots (5.10)$$

$$\tilde{B} = 1 + \frac{3}{2} \left[\frac{\epsilon \cos \varphi_1 + b(\varphi_1)}{h_o(\varphi_1)} \right]^2$$

For the problem of small radial displacement, assume

$$\tilde{g}_1(\varphi) = \tilde{u}(\varphi) + i\tilde{v}(\varphi) \dots \dots \dots (5.11)$$

The governing equations for $\tilde{u}(\varphi)$ and $\tilde{v}(\varphi)$ are Eqs. (4.2) and (4.3) replacing u and v by \tilde{u} and \tilde{v} respectively. The boundary conditions are however

$$\tilde{u}(\varphi_i) = 3 h_1(\varphi_i) \left\{ h_o^2(\varphi_i) + \frac{1}{2} \left[\epsilon \cos \varphi_i + b(\varphi_i) \right]^2 \right\} \quad (i = 1, 2) \dots \dots \dots (5.12)$$

$$\tilde{v}(\varphi_i) = 0$$

The results of the numerical analysis in Appendix II are also applicable if appropriate boundary conditions (Eq. (5.12)) are used.

The following special cases of mode shape of gap oscillations are of interest:

1.) $b(\varphi) \equiv 0$

Structural flexibility is negligible. Gap oscillation is solely caused by axial excursion of the bearing as a rigid body. This is the case studied in Sections 2, 3 and 4.

2.) $\epsilon = 0, b(\varphi) = \text{constant}.$

This represents a mode of uniform normal oscillations of the bearing surface.

Various combinations of ϵ and $b = \text{constant}$ can approximate quite well the actual squeeze motion of the bearing surface, including the influence of structural flexibility. The analysis in this section, however, is valid for any mode shape of the squeeze motion of the bearing surface.

6. RESULTS

The axial load and stiffness of a concentric ($\eta_z = 0$) hemi-spherical squeeze-film ($\phi_1 = 0^\circ, \phi_2 = 90^\circ$) have been calculated and are graphically shown in Fig. 2. These curves can be used as a preliminary guide for estimating the load requirements of a spherical squeeze-film thrust bearing. The need for sufficient amplitude of the squeeze motion is clearly indicated. For $\epsilon < 0.4$, every increment of 0.1 in ϵ at least doubles the load capacity. Gain in the stiffness with increased ϵ is even larger.

In Figs. 3 through 5 are the axial load capacity and stiffness for a bearing geometry being tested at the Astrionics Laboratory ($\phi_1 = 0, \phi_2 = 67^\circ$). The normal way in presenting these results is done in Fig. 3. Because the unit load in the actual test is typically very small, the magnitude of the axial displacement is considerably larger than the nominal bearing clearance. Under this condition, the mean gap at the pole of the bearing, $C(1 + \eta)$, is more representative of the fluid film thickness than the nominal gap, C . For this reason, the normalized variables are rescaled and the results are shown in Fig. 4 and 5. Both the load capacity and the stiffness, in terms of rescaled normalized variables, increase with η ; this is because the bearing gap becomes smaller toward ϕ_2 for larger η . However, as η_z becomes larger and larger, the curves appear to approach some asymptotes as may be expected.

Calculations of both axial and radial displacement effects have been made for the geometry corresponding to $\phi_1 = 41.5^\circ, \phi_2 = 68^\circ$. This geometry is of interest because it circumscribes the "iso-elastic cone". (The "iso-elastic" cone has an apex angle equal to $2 \tan^{-1} (1/\sqrt{2})$. If the local normal spring rate over such a cone is uniform, its over-all axial and radial stiffnesses are equal). Axial forces, axial stiffness, and radial stiffness are respectively shown in Figs. 6, 7 and 8. for the non-rotating squeeze-film bearing. (There is no tangential stiffness in this case). Comparing with Fig. 2, it is seen that the axial load is about 15% lower than that of the hemi-spherical bearing, while the axial stiffness is about 50% lower. Comparing Figs. 7 and 8, it is seen that the radial stiffness is somewhat smaller than the axial stiffness. Thus, to achieve iso-elasticity, ϕ_2 would have to be larger. The effects of journal rotation are illustrated in Figs. 9 through 12. In Figs. 9 and 10, radial and tangential stiffnesses for $\epsilon = 0.5$ are shown. It is seen that the rotational effects can be neglected for $\Lambda < 2$, whereas substantial increase in the radial stiff-

ness over the squeeze-film bearing (without rotation) for $\Lambda > 50$, is caused by rotation. In Figs. 11 and 12, radial and tangential stiffnesses of the concentric squeeze-film hybrid bearing are plotted against the excursion ratio (for the axial squeeze-motion) for various values of Λ (rotational or self-acting effect). It is seen that for each Λ , the radial stiffness increases with ϵ and approaches essentially to that of the non-rotating squeeze-film bearing when ϵ is sufficiently large. For instance, at $\Lambda = 10$, the radial stiffness is very close to that of the non-rotating squeeze-film bearing for $\epsilon > 0.4$; whereas at $\Lambda = 100$, the corresponding transition appears to be beyond $\epsilon = 1.0$. The radial stiffness of the hybrid squeeze-film bearing is approximately equal to the sum of those due to squeeze-film and rotational effects separately. The curves for the tangential stiffness show that the contribution of the squeeze-film motion is essentially negligible.

7. CONCLUSIONS

According to the analysis and the sample results considered in the previous sections, the following conclusions can be drawn:

a. The asymptotic analysis of squeeze-film bearings is applicable when σ is sufficiently large. According to the asymptotic analysis, $\psi = PH$ is time independent. The error involved in the asymptotic analysis concerning the bearing load capacity is of the order of $1/\sqrt{\sigma}$.

b. Up to the first order of the radial displacement, the axial load capacity and the axial stiffness are independent of the radial displacement and the journal rotation.

c. When the mean gap is much larger than the nominal gap due to a large axial displacement, (for a bearing consisting of primarily the polar region), the nominal gap dimension has little significance. In the case, the mean gap at the pole becomes the appropriate reference dimension for the bearing gap.

d. The hybrid squeeze-film bearing has a radial stiffness approximately equal to the sum of these due to squeeze-film and rotational effects separately.

e. The tangential stiffness of the hybrid squeeze-film bearing is practically independent of the squeeze-film motion.

ACKNOWLEDGEMENT

The authors wish to thank Miss M. Denise Creeden for carrying out the programming.

REFERENCES

1. Salbu, E.O.J., "Compressible Squeeze-Film and Squeeze Bearings", Trans ASME, J. of Basic Engineering, Vol. 86, Series D, No.2, p. 355, June 1964.
2. Pan, C.H.T., Editor, "Analysis, Design and Prototype Development of Squeeze-Film Bearings for AB-5 Gyro", MTI Report 64-TR-66, November, 1964.
3. Pan, C.H.T., "Gas Lubricated Spherical Bearings", Trans. ASME, J. of Basic Engineering, Vol. 85, Series D, No. 2, p. 311, June 1963.
4. Pan, C.H.T., "Thrust Capability of Isothermal Spherical Squeeze-Film Bearing", MTI 65-TM-5, March 1965.
5. Pan, C.H.T., "On Asymptotic Analysis of Gaseous Squeeze-Film Bearings", MTI 65TR 20, April, 1965.
6. Peirce, B.O., "A Short Table of Integrals", Ginn and Company, 1956.

APPENDIX I

SPECIAL SOLUTIONS FOR THE AXIALLY SYMMETRIC PROBLEM

Analytical expressions for the mean axial load and mean axial stiffness are obtained for four special cases; they are

- a) $\varphi_1 > 0^\circ$
- b) $\varphi_1 = 0^\circ$
- c) $\varphi_1 = 0^\circ, \eta_z = 0$
- and d) $\varphi_1 = 0^\circ, \eta_z = 0, \varphi_2 = 90^\circ$.

Case a) $\varphi_1 > 0^\circ$

Use Eq. (3.11) for the mean axial load with

$$\psi_\infty(\varphi) = \left\{ A h_o^2(\varphi) I(\varphi) + \left[\frac{h_o(\varphi)}{h_o(\varphi_1)} \right]^2 \psi_\infty^2(\varphi_1) \right\}^{\frac{1}{2}} \dots \dots \dots (I.1)$$

$$I(\varphi) = J(\varphi) - J(\varphi_1) \dots \dots \dots (\varphi \geq \varphi_1 \geq \varphi_1) \dots \dots \dots (I.2)$$

$$J(\varphi) = \beta_1 \log_e \left| 1 + \cos\varphi \right| + \beta_2 \log_e \left| 1 - \cos\varphi \right| + \beta_3 \log_e \left| 1 + \eta_z \cos\varphi \right| + \beta_4 / (1 + \eta_z \cos\varphi) + \beta_5 / (1 + \eta_z \cos\varphi)^2 \dots \dots \dots (I.3)$$

and

$$\left. \begin{aligned} \beta_1 &= \frac{1}{2(\eta_z - 1)^3} , \\ \beta_2 &= \frac{1}{2(\eta_z + 1)^3} , \\ \beta_3 &= -(\beta_1 + \beta_2) , \\ \beta_4 &= (3 - \eta_z) \beta_1 + (3 + \eta_z) \beta_2 + 2\beta_3 , \\ \beta_5 &= \frac{1}{2} \left[3(1 - \eta_z) \beta_1 + 3(1 + \eta_z) \beta_2 + (1 - \eta_z^2) \beta_3 + \beta_4 \right] \end{aligned} \right\} \dots \dots \dots (I.4)$$

Eq. (3.11) can then be integrated numerically. (Simpson's quadrature formula is used).

The mean axial stiffness is obtained numerically by calculating the mean axial load, Eq. (3.11) at small increments around the actual axial eccentricity ratio. Thus,

$$\frac{Ck_z}{\pi p_a R^2} = \frac{1}{2 \Delta \eta_z} \left\{ \frac{F_z^{(+)}}{\pi p_a R^2} - \frac{F_z^{(-)}}{\pi p_a R^2} \right\}, \quad \dots \quad (I.5)$$

where superscripts (+), (-) refer to $+\Delta\eta$ and $-\Delta\eta$ respectively. A suitable value for $\Delta\eta$ is 0.01.

Case b) $\varphi_1 = 0^\circ$

$$\frac{F_z}{\pi p_a R^2} = EI_1 + \frac{1}{2} [\cos 2\varphi_2 - 1], \quad \dots \quad (I.6)$$

$$\text{where } E = \frac{1}{\sqrt{1 + \frac{3/2 \epsilon^2 \cos^2 \varphi_2}{(1+\eta_z \cos \varphi_2)^2}}}, \quad \dots \quad (I.7)$$

$$\text{and } I_1 = \int_0^{\varphi_2} \frac{\sin 2\varphi (1+\eta_z \cos \varphi) d\varphi}{\sqrt{(1+\eta_z \cos \varphi)^2 - \epsilon^2 \cos^2 \varphi}} \quad \dots \quad (I.8)$$

$$\frac{Ck_z}{\pi p_a R^2} = -\frac{\partial}{\partial \eta_z} \left(\frac{F_z}{\pi p_a R^2} \right) = - \left[I_1 \frac{\partial E}{\partial \eta_z} + E I_2 \right], \quad \dots \quad (I.9)$$

$$\text{where } \frac{\partial E}{\partial \eta_z} = -\frac{3/2 \epsilon^2 \cos^3 \varphi_2}{(1+\eta_z \cos \varphi_2)^3 E}, \quad \dots \quad (I.10)$$

$$\text{and } I_2 = -\epsilon^2 \int_0^{\varphi_2} \frac{\sin 2\varphi \cos^3 \varphi d\varphi}{[(1+\eta_z \cos \varphi)^2 - \epsilon^2 \cos^2 \varphi]^{3/2}} \quad \dots \quad (I.11)$$

Case c $\varphi_1 = 0^\circ, \eta_z = 0$

$$\frac{F_z}{\pi p_a R^2} = E_0 I_{10} + \frac{1}{2} [\cos 2\varphi - 1] \quad \dots \quad (I.12)$$

$$\text{where } E_0 = \frac{1}{\sqrt{1 + \frac{3}{2} \epsilon^2 \cos^2 \varphi_2}} \quad \dots \quad (I.13)$$

$$\text{and } I_{10} = \int_0^{\varphi_2} \frac{\sin 2\varphi d\varphi}{\sqrt{1 - \epsilon^2 \cos^2 \varphi}} = \frac{2}{\epsilon^2} \left[(1 - \epsilon^2 \cos^2 \varphi_2)^{\frac{1}{2}} - (1 - \epsilon^2)^{\frac{1}{2}} \right] \quad \dots \quad (I.14)$$

$$\frac{Ck_z}{\pi p_a R^2} = - \left[I_{10} \frac{\partial E_0}{\partial \eta_z} + E_0 I_{20} \right] \quad \dots \quad (I.15)$$

$$\text{where } \frac{\partial E_o}{\partial \eta_z} = -\frac{3}{2} \epsilon^2 \frac{\cos^3 \varphi_2}{E_o} \dots \dots \dots (I.16)$$

$$\begin{aligned} \text{and } I_{20} = & -\epsilon^2 \int_0^{\varphi_2} \frac{\sin 2\varphi \cos^3 \varphi d\varphi}{[1-\epsilon^2 \cos^2 \varphi]^{3/2}} = 2 \left[(1-\epsilon^2 \cos^2 \varphi_2)^{-\frac{1}{2}} \cos^3 \varphi_2 - (1-\epsilon^2)^{-\frac{1}{2}} \right] \\ & + \frac{6}{\epsilon^2} \left[(1-\epsilon^2 \cos^2 \varphi_2)^{\frac{1}{2}} \cos \varphi_2 - (1-\epsilon^2)^{\frac{1}{2}} \right] - \frac{3}{\epsilon} \left[\gamma + \frac{1}{2} \sin^2 \gamma \right]_{\gamma_1}^{\gamma_2} \end{aligned} \quad (I.17)$$

$$\text{where } \gamma_2 = \arcsin(\epsilon \cos \varphi_2), \gamma_1 = \arcsin(\epsilon). \dots \dots \dots (I.18)$$

Case c) $\varphi_1 = 0^\circ, \eta_z = 0, \varphi_2 = 90^\circ$

$$\frac{F_z}{\pi p_a R^2} = \frac{2}{\epsilon^2} \left[1 - (1-\epsilon^2)^{\frac{1}{2}} \right] - 1 \dots \dots \dots (I.19)$$

$$\begin{aligned} \frac{Ck_z}{\pi p_a R^2} = & 2 \left[1 - \epsilon^2 \right]^{-\frac{1}{2}} + \frac{6}{\epsilon^2} \left[1 - \epsilon^2 \right]^{\frac{1}{2}} - \frac{3}{\epsilon} \left\{ \arcsin(\epsilon) \right. \\ & \left. + \frac{1}{2} \sin 2 \left(\arcsin(\epsilon) \right) \right\} \dots \dots \dots (I.20) \end{aligned}$$

APPENDIX II

NUMERICAL INTEGRATION OF SYSTEM (4.2), (4.3) AND (4.4) USING INFLUENCE COEFFICIENT METHOD

Denoting $u' = \frac{du}{d\varphi}$ and $v' = \frac{dv}{d\varphi}$, Equation (4.2) and (4.3) can be written as a system of first order differential equations. Using matrix notation, we have:

$$\begin{bmatrix} A_{11} & 0 & A_{13} & A_{14} \\ 0 & A_{22} & -A_{14} & A_{13} \\ 1 & 0 & -\frac{d}{d\varphi} & 0 \\ 0 & 1 & 0 & -\frac{d}{d\varphi} \end{bmatrix} \begin{bmatrix} u' \\ v' \\ u \\ v \end{bmatrix} = \begin{bmatrix} B_1 \\ B_2 \\ 0 \\ 0 \end{bmatrix} \dots \dots \dots (II.1)$$

where

$$\begin{aligned} A_{11} &= A_{22} = \frac{d}{d\varphi} + \left(\operatorname{ctn}\varphi + \frac{3\eta_z \sin\varphi}{1+\eta_z \cos\varphi} \right) \\ A_{13} &= 3\eta_z \left[\frac{2\cos\varphi}{1+\eta_z \cos\varphi} + \frac{\eta_z \sin^2 \varphi}{(1+\eta_z \cos\varphi)^2} \right] - \csc^2 \varphi \\ A_{14} &= \frac{\Lambda}{(1+\eta_z \cos\varphi)\sqrt{G_o}} \\ B_1 &= \frac{3}{\sin\varphi(1+\eta_z \cos\varphi)^3} \left\{ g_o \left[(\eta_z + \cos\varphi)^2 + \sin^2 \varphi (\eta_z^2 - 1) \right] + \frac{dg_o}{d\varphi} \sin\varphi (1+\eta_z \cos\varphi) \right. \\ &\quad \left. (\eta_z + \cos\varphi) \right\} - 3 \frac{G_o}{\sin\varphi} \\ B_2 &= -\Lambda \frac{\sin^3 \varphi}{1+\eta_z \cos\varphi} \sqrt{G_o} \end{aligned} \quad (II.2)$$

The boundary conditions to be satisfied by (II.1) are, from Eq.(4.4)

$$\begin{aligned} u(\varphi_1) &= 3 \sin\varphi_1 \left[(1 + \eta_z \cos\varphi_1)^2 + \frac{1}{2} \epsilon^2 \cos^2 \varphi_1 \right] \\ u(\varphi_2) &= 3 \sin\varphi_2 \left[(1 + \eta_z \cos\varphi_2)^2 + \frac{1}{2} \epsilon^2 \cos^2 \varphi_2 \right] \\ v(\varphi_1) &= 0 \\ v(\varphi_2) &= 0 \end{aligned} \quad \dots \dots \dots (II.3)$$

Let Eq.(II.1) be abbreviated in the form

$$\bar{A} \bar{w} = \bar{B} \quad \dots \dots \dots (II.4)$$

and its solution can be written as

$$\bar{w} = \bar{w}_p + c_1 \bar{w}_1 + c_2 \bar{w}_2 + u(\varphi_1) \bar{w}_3 + v(\varphi_1) \bar{w}_4 \quad \dots \dots \dots (II.5)$$

where c_1 and c_2 are undetermined constants. In Eq.(II.5) \bar{w}_p is the particular solution of (II.4), satisfying homogeneous initial conditions,

$$\bar{w}_p(\varphi_1) = \begin{bmatrix} 0 \\ 0 \\ 0 \\ 0 \end{bmatrix} \quad \dots \dots \dots (II.6)$$

whereas \bar{w}_1 , \bar{w}_2 and \bar{w}_3 are to be solved from the homogeneous equation

$$\bar{A} \bar{w} = 0 \quad \dots \dots \dots (II.7)$$

with respective initial conditions,

$$\bar{w}_1(\varphi_1) = \begin{bmatrix} 1 \\ 0 \\ 0 \\ 0 \end{bmatrix} ; \quad \bar{w}_2(\varphi_1) = \begin{bmatrix} 0 \\ 1 \\ 0 \\ 0 \end{bmatrix} ; \quad \bar{w}_3(\varphi_1) = \begin{bmatrix} 0 \\ 0 \\ 1 \\ 0 \end{bmatrix} \quad \dots \dots \dots (II.8)$$

The last term of Equation (II.5) can be disregarded since $v(\varphi_1) = 0$. It is not difficult to show that the elements of w_1 and w_2 are related in the following manner:

$$\left. \begin{array}{l} u_2' = -v_1' \\ v_2' = u_1' \\ u_2 = -v_1 \\ v_2 = u_1 \end{array} \right\} \quad \dots \dots \dots (II.9)$$

Hence, it is only necessary to solve for either \bar{w}_1 or \bar{w}_2 .

The solutions \bar{w}_p , \bar{w}_1 , and \bar{w}_3 , can be obtained by the Runge-Kutta method of numerical integration. A standard subroutine is available in the computer library.

Knowing these solutions, the constants c_1 and c_2 can be determined from the boundary conditions

$$\left. \begin{aligned} u(\varphi_2) &= u_p(\varphi_2) + c_1 u_1(\varphi_2) + c_2 [-v_1(\varphi_2)] + u(\varphi_1) u_3(\varphi_2) \\ v(\varphi_2) &= v_p(\varphi_2) + c_1 v_1(\varphi_2) + c_2 [u_1(\varphi_2)] + u(\varphi_1) v_3(\varphi_2) \end{aligned} \right\} \dots \dots \dots (II.10)$$

Solving for c_1 and c_2 we find

$$\left. \begin{aligned} c_1 &= \frac{1}{D} \left\{ u_2(\varphi_2) [v_p(\varphi_2) + u(\varphi_1) v_3(\varphi_2)] + v_2(\varphi_2) [u(\varphi_2) - u_p(\varphi_2) - u(\varphi_1) u_3(\varphi_2)] \right\} \\ c_2 &= \frac{1}{D} \left\{ -u_1(\varphi_2) [v_p(\varphi_2) + u(\varphi_1) v_3(\varphi_2)] - v_1(\varphi_2) [u(\varphi_2) - u_p(\varphi_2) - u(\varphi_1) u_3(\varphi_2)] \right\} \end{aligned} \right\} (II.11)$$

where $D = u_1(\varphi_2) v_2(\varphi_2) - v_1(\varphi_2) u_2(\varphi_2)$

$$= [u_1(\varphi_2)]^2 + [v_1(\varphi_2)]^2 \dots \dots \dots (II.12)$$

Thus the solutions, u and v , are readily obtained from Eq. (II.5).

$$\left. \begin{aligned} u &= u_p + c_1 u_1 + c_2 (-v_1) + u(\varphi_1) u_3 \\ v &= v_p + c_1 v_1 + c_2 (u_1) + u(\varphi_1) v_3 \end{aligned} \right\} \dots \dots \dots (II.13)$$

NOMENCLATURE

A, B	Integration constant.
\bar{A}	Coefficient matrix as defined in Eq. (II 4)
b	A function of Φ , representing gap oscillation in Eq. (5.1).
C	Bearing radial clearance.
c_1, c_2	Arbitrary constants in Eq. (II.5).
e	Excursion amplitude.
e_r, e_z	Radial and axial displacement; e_z is positive when journal is moving away from bearing.
$F()$	Bearing force in the direction of ().
g_o, g_1	Defined in (2.28).
G_o	Defined in (3.2).
h_o, h_1	Defined in (2.31) and (2.32).
H	Normalized film thickness.
H_o	Temporal average of H .
H	Normalized film thickness with structure vibrations taken into account.
I	Defined in (2.20).
$k()$	Stiffness in the direction of ().
p	Pressure
P	Normalized pressure, p/p_a .
R	Radius.
Re	Real part.
t	Time.
u, v	Real and imaginary parts of g .
\bar{w}	u', v', u, v as defined in Eq. (II.4)
α	Attitude angle.
ϵ	e/C , dimensionless excursion ratio.
η_r	$\frac{e_r}{C}$, dimensionless radial displacement ratio.
η_z	$\frac{e_z}{C}$, dimensionless axial displacement ratio.
θ	Meridian angle.
$\bar{\theta}$	$\theta - \alpha$
ρ	Density.
φ	Azimuthal angle.

$$\Lambda = \frac{6\mu\omega}{p_a} \left(\frac{R}{C} \right)^2 = \text{Compressibility number}$$

μ Viscosity

$$\sigma = \frac{12 \mu \Omega}{p_a} \left(\frac{R}{C} \right)^2 = \text{Squeeze number.}$$

\bar{t} Ωt , dimensionless time.

ψ PH

ψ_∞ Asymptotic approximation of ψ .

ω Meridional angular speed of rotation.

Ω Squeeze frequency.

Subscripts

a Ambient

e Edge

R Radial

T Tangential

Z Axial

1 Refers to ϕ_1 .

2 Refers to ϕ_2 .

Superscripts

\sim With structural vibrations.

LIST OF FIGURES

- Fig. 1 Spherical Squeeze-Film Bearing.
- " 2 Unit Axial Load and Stiffness vs. Axial Excursion Ratio for
a Concentric, Hemispherical, Axial-Squeeze Film Bearing.
- " 3 Unit Axial Load and Stiffness vs. Axial Eccentricity Ratio for
Various Excursion Ratios.
- " 4 Unit Axial Load vs. Excursion Ratio (effective)
- " 5 Unit Axial Stiffness vs. Excursion Ratio (effective).
- " 6 Unit Axial Load Capacity vs. Excursion Ratio for Various
Axial Displacement Ratio.
- " 7 Unit Axial Stiffness vs. Excursion Ratio for Various Axial
Displacement Ratio.
- " 8 Unit Radial Stiffness vs. Excursion Ratio for Various Axial
Displacement Ratio.
- " 9 Unit Radial Stiffness vs. Λ for Various Axial Displacement Ratio.
- " 10 Unit Tangential Stiffness vs. Λ for various Axial Displacement Ratio.
- " 11 Unit Radial Stiffness vs. Excursion Ratio for Various Λ .
- " 12 Unit Tangential Stiffness vs. Excursion Ratio for Various Λ .

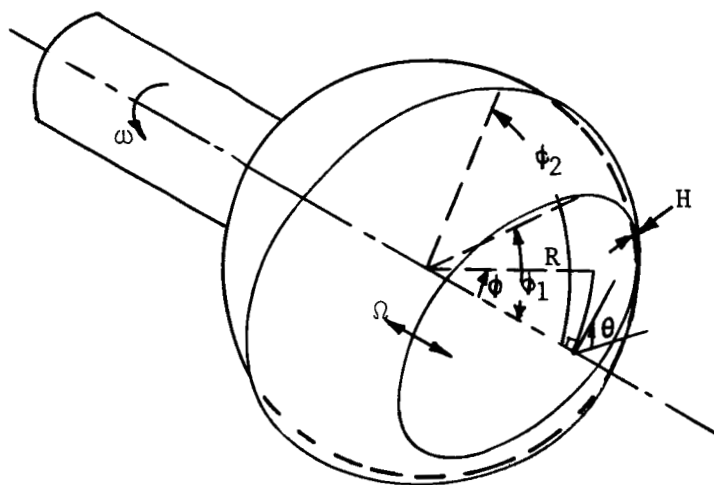


Fig. 1 Spherical Squeeze-Film Bearing

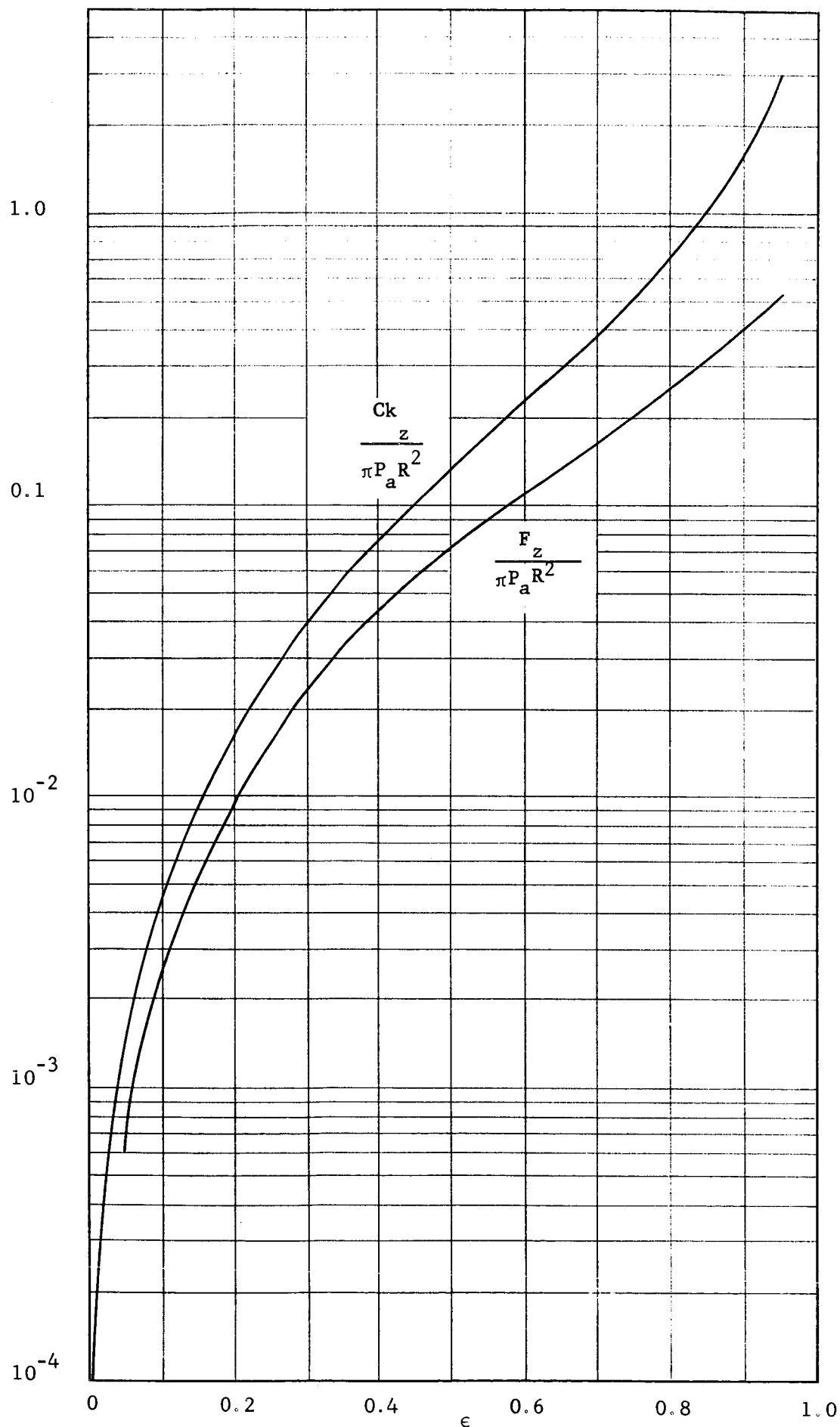


Fig. 2 Unit axial load and stiffness vs. axial excursion ratio for a concentric, hemispherical, axial-squeeze film bearing.

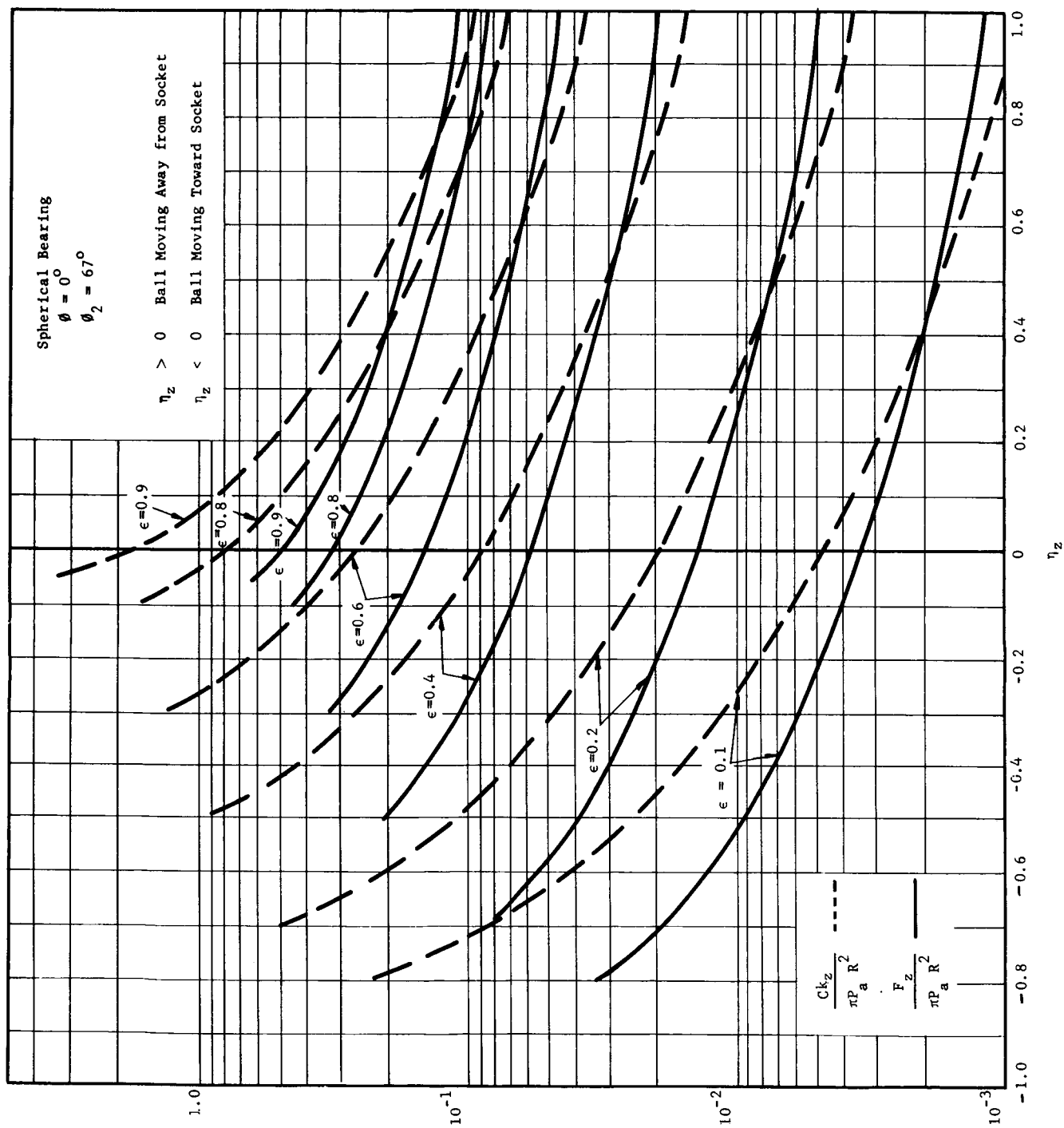


Fig. 3 Unit Axial Load and Stiffness Versus Axial Eccentricity Ratio for Various Excursion Ratios

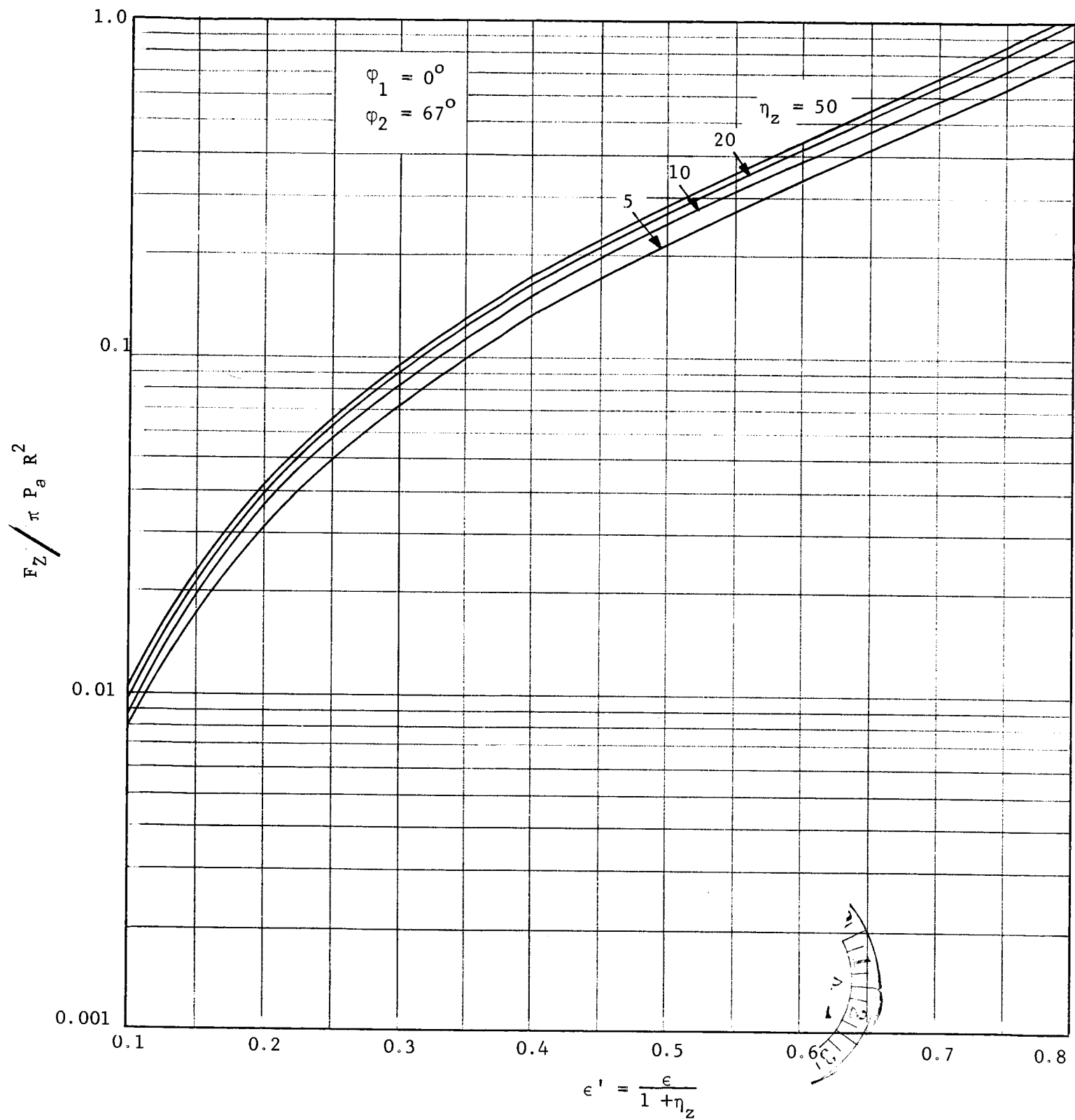


Fig. 4 Unit axial load vs. excursion ratio (effective).

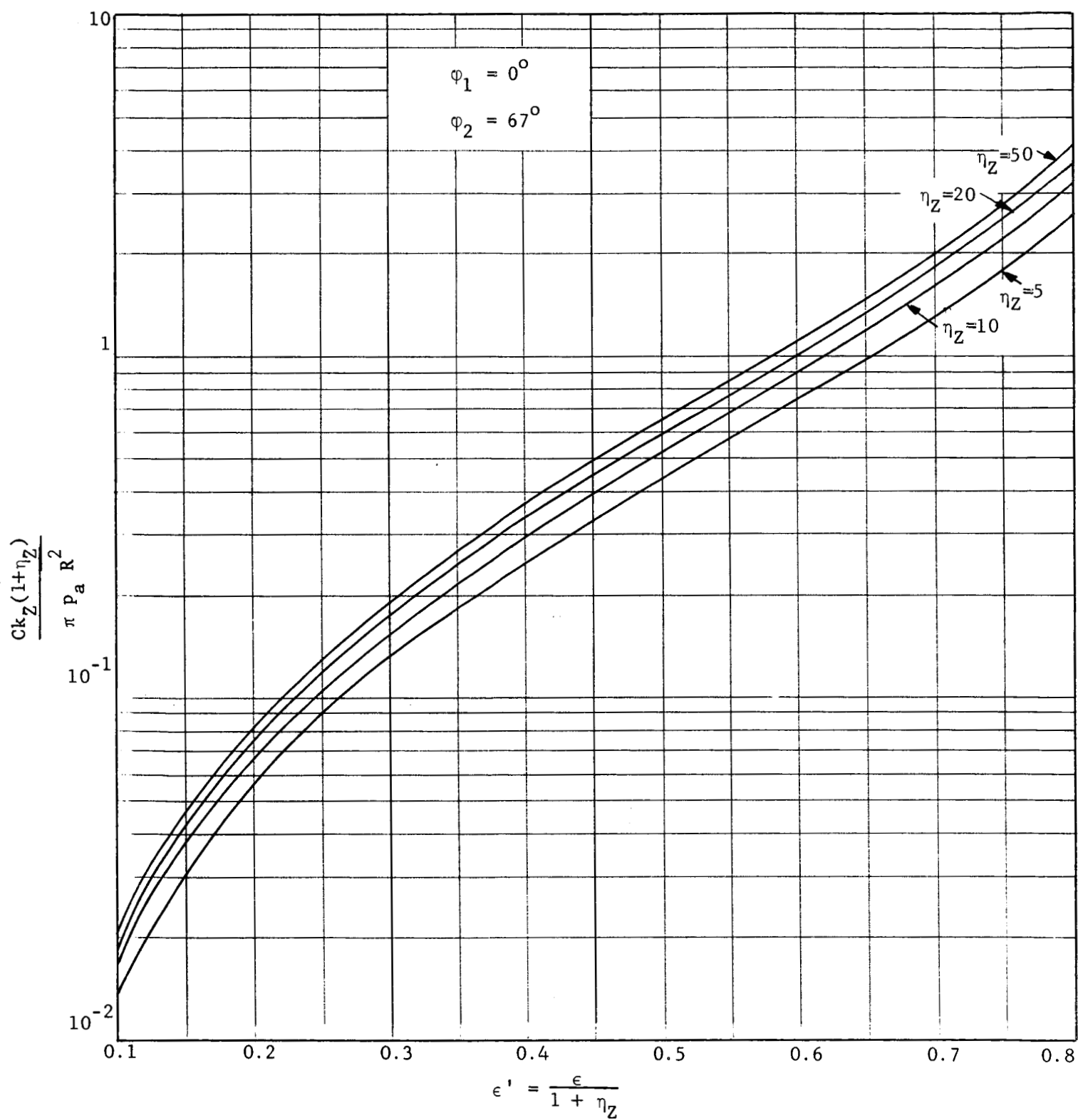


Fig. 5 Unit Axial Stiffness Versus Excursion Ratio (Effective)

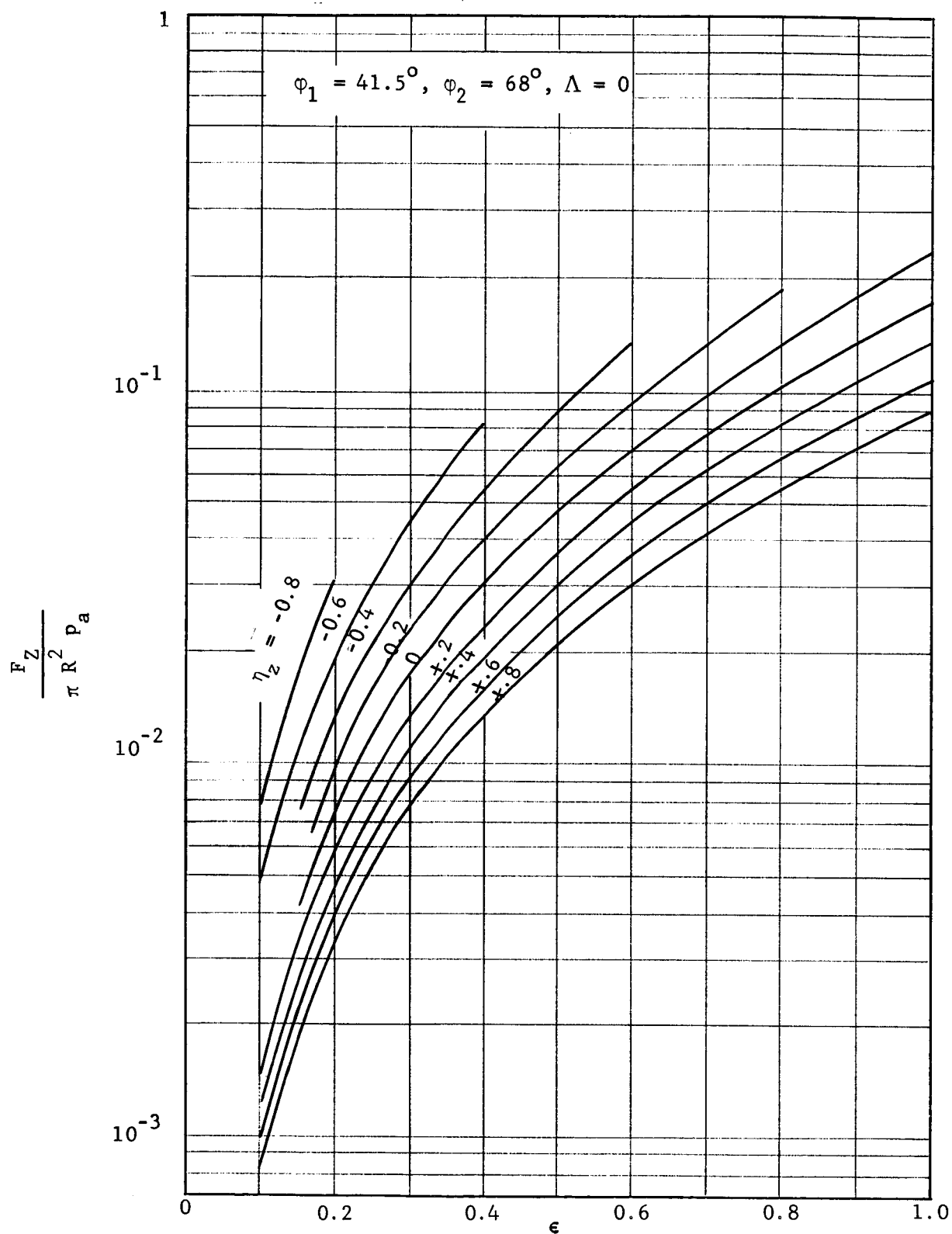


Fig. 6 Unit axial load capacity vs. excursion ratio for various axial displacement ratio.

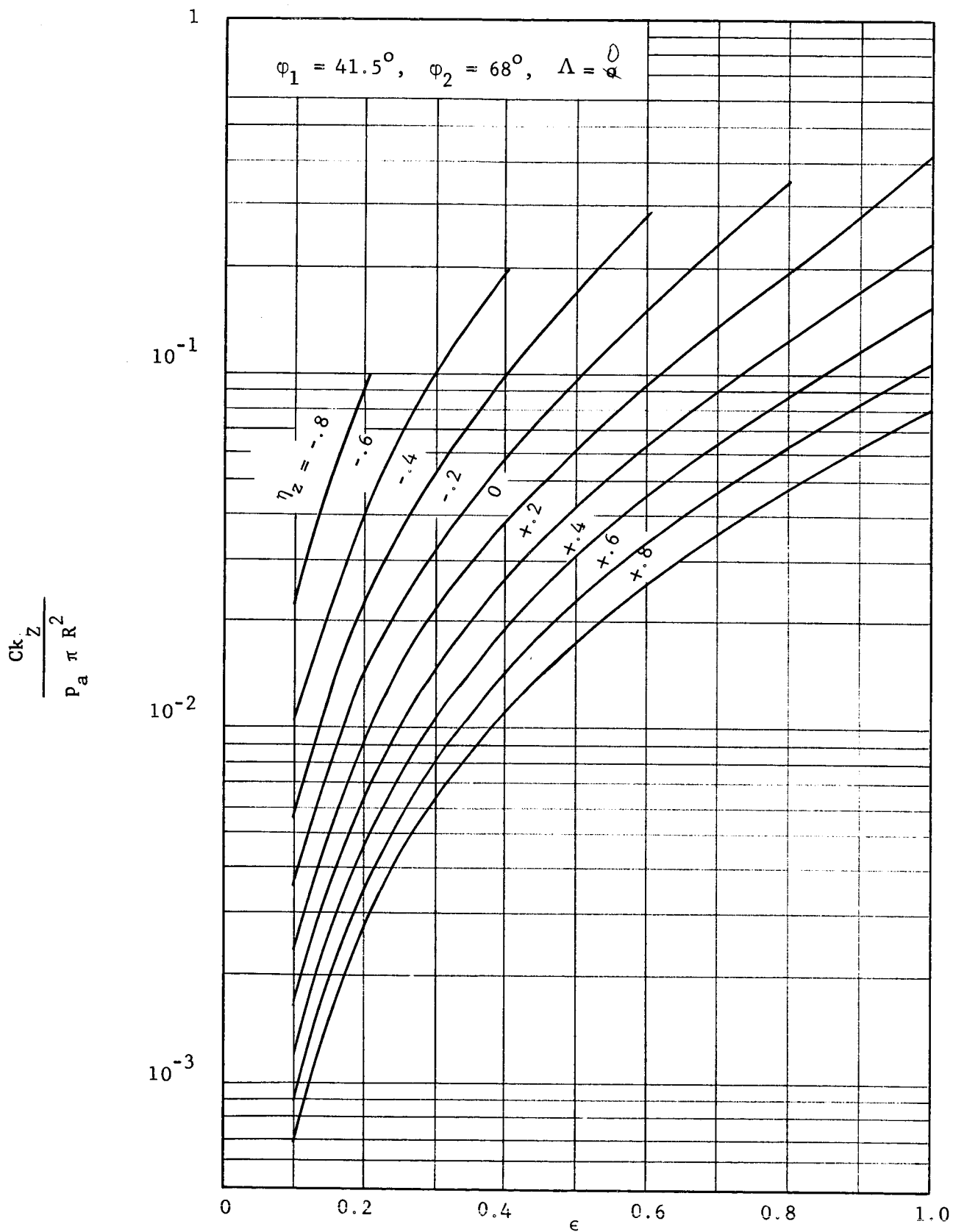


Fig. 7 Unit axial stiffness vs. excursion ratio for various axial displacement ratio.

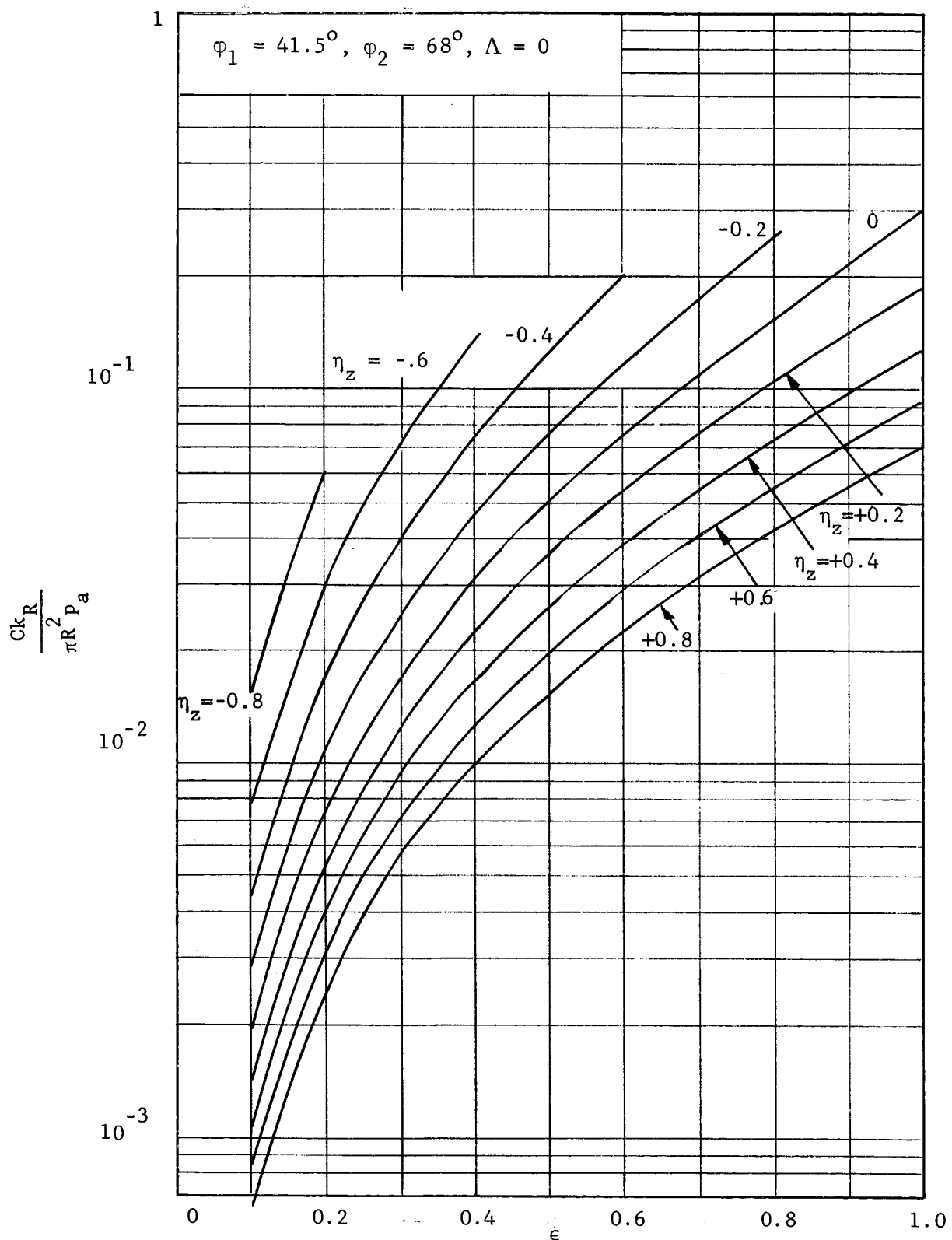


Fig. 8 Unit Radial Stiffness vs. Excursion Ratio for various axial displacement ratio.

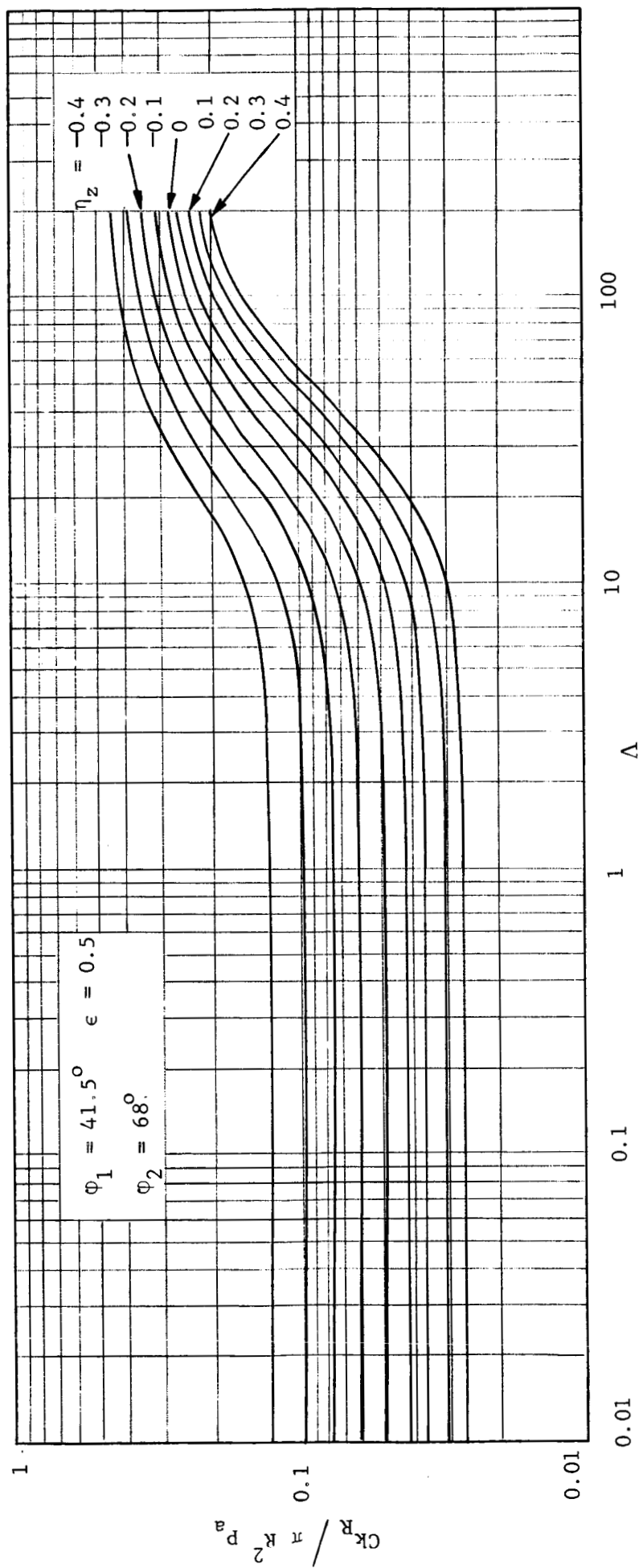


Fig. 9 Unit Radial Stiffness vs. Δ for various axial displacement ratio.

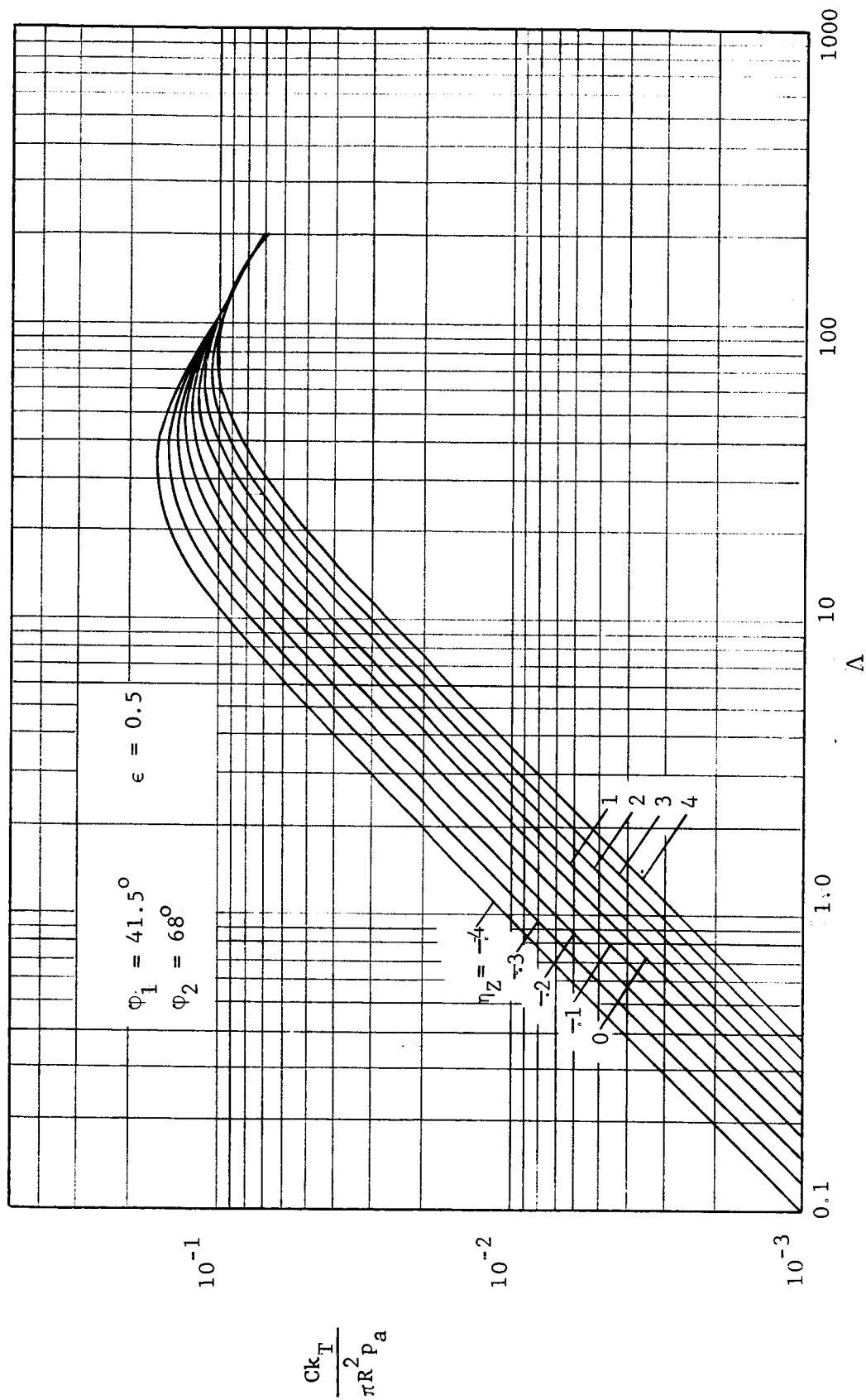


Fig. 10 Unit tangential stiffness vs. Δ for various axial displacement ratio.

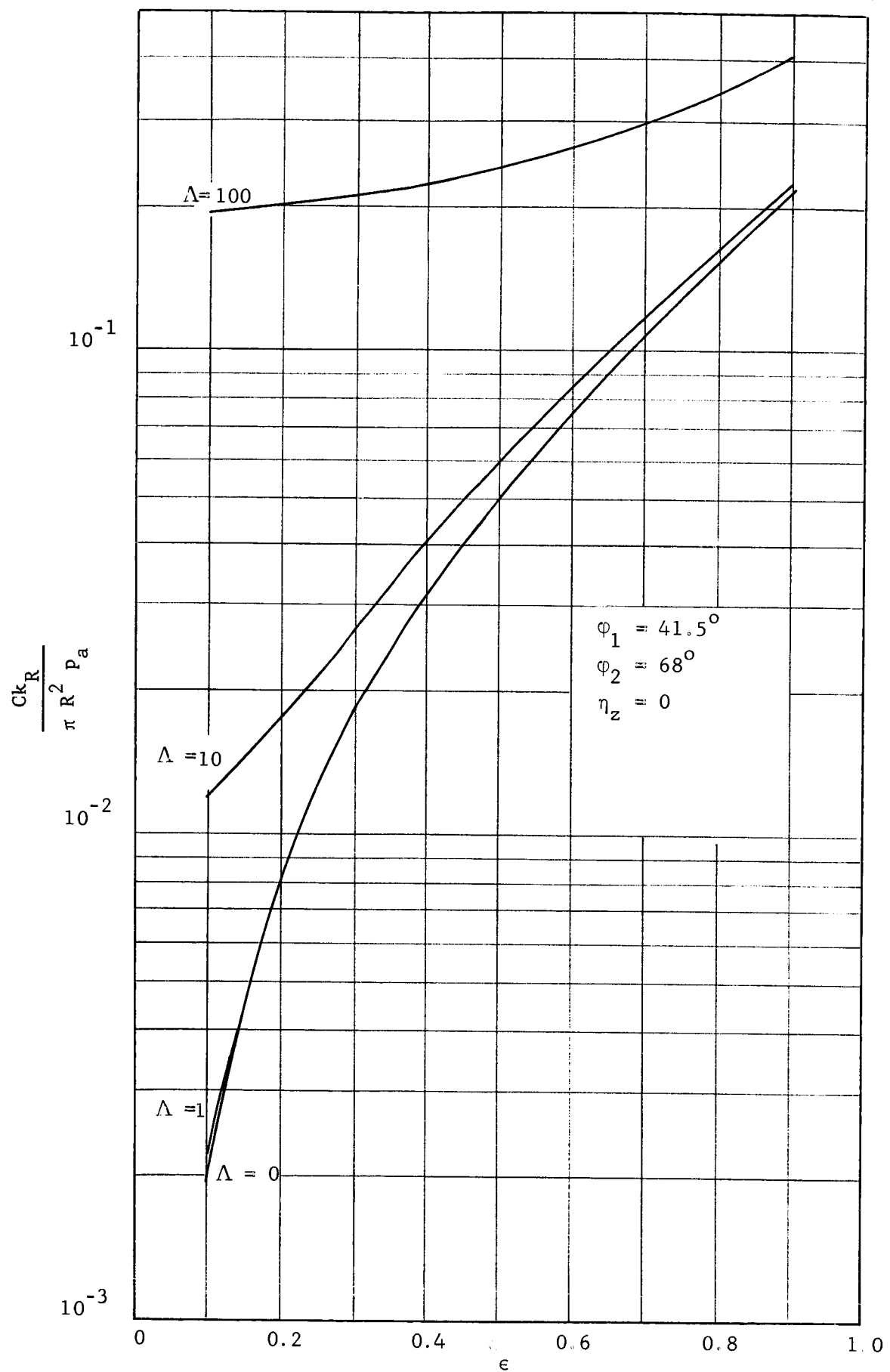


Fig. 11 Unit radial stiffness versus excursion ratio for various Λ .

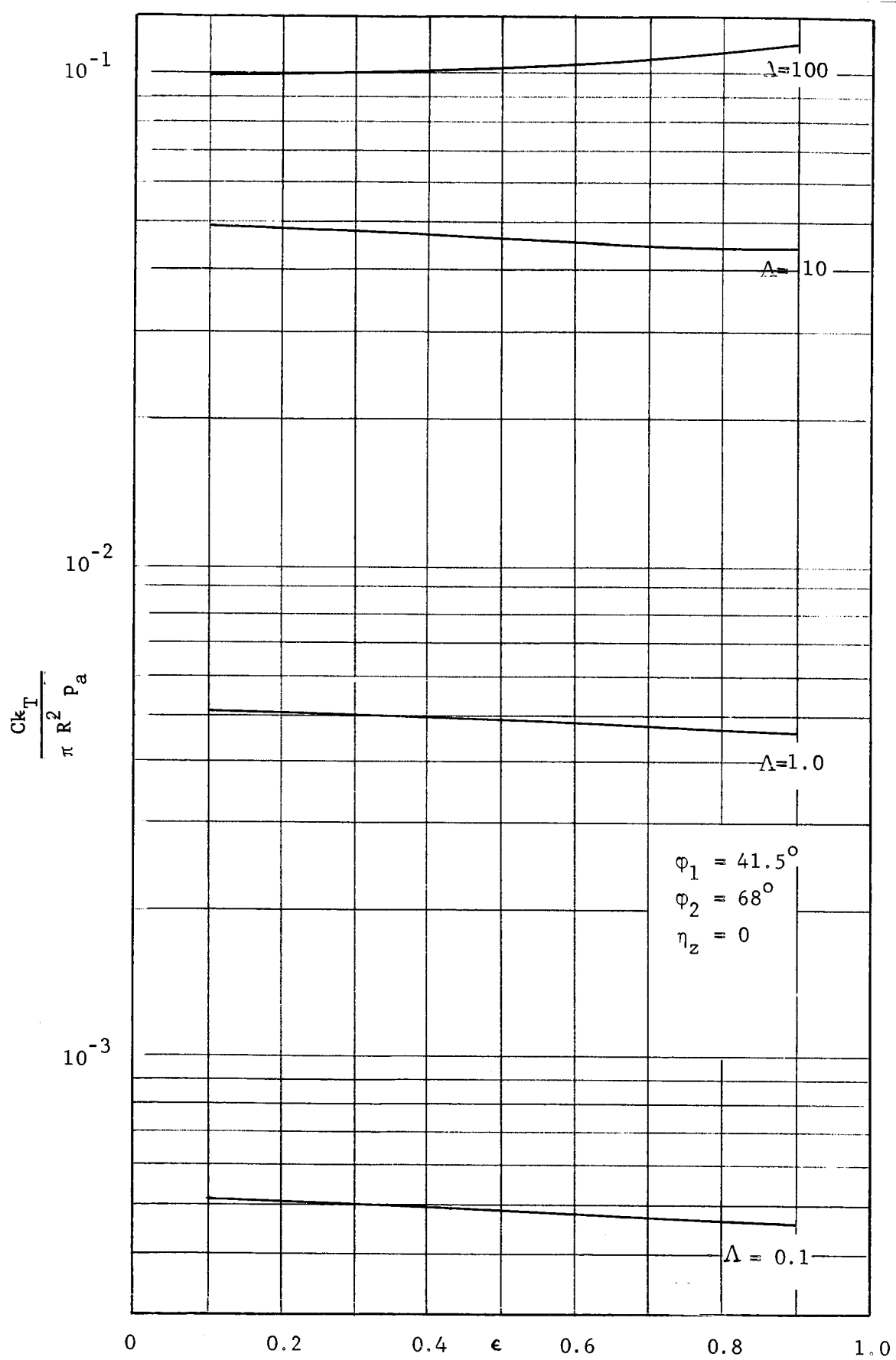


Fig. 12 Unit tangential stiffness versus excursion ratio for various Λ .